University of Southern Queensland

Faculty of Engineering and Surveying

Behaviour and Design of Connections in Modular Steel Buildings

A dissertation submitted by

Matthew Trent

In fulfillment of the requirements of

ENG4111 and ENG4112 Research Project

Towards the degree of

Bachelor of Engineering (Honours) (Civil)

October 2023

Abstract

Connections or joints are the fundamental components that bring together individual three-dimensional volumetric modules to form a complete modular building. Due to the discontinuous nature of corner-supported modular buildings, high concentrations of stress develop within the connections. The structural capacity of connections should be well defined to effectively create a continuous structural building system. However, the design of reliable intermodular connection remains a significant challenge. This research reviews and remodels two proposed connection models and combines the two selected intermodular connections to create an innovative individual intermodular connection model. The modelling has been completed through numerical simulation in the FEA software ABAQUS v.2019 to reveal and compare the behaviour of the three proposed intermodular connection models. The simulation has been conducted across a range of loading scenarios to compare and determine the behaviour of the intermodular connections. The numerical analyses revealed an improved response for the novel intermodular connection model under all applied loading scenarios. This study has shown that the combination of interlocking plates, shear keys and a post tensioned rod can significantly improve the IMCs performance under a range of loading applications.

University of Southern Queensland

Faculty of Health, Engineering & Sciences

ENG4111/2 Research Project

Limitations of Use

The Council of the University of Southern Queensland, its Faculty of Health, Engineering & Sciences, and the staff of the University of Southern Queensland, do not accept any responsibility for the truth, accuracy or completeness of material contained within or associated with this dissertation.

Persons using all or any part of this material do so at their own risk, and not at the risk of the Council of the University of Southern Queensland, its Faculty of Health, Engineering & Sciences or the staff of the University of Southern Queensland.

This dissertation reports an educational exercise and has no purpose or validity beyond this exercise. The sole purpose of the course pair entitled "Research Project" is to contribute to the overall education within the student's chosen degree program. This document, the associated hardware, software, drawings, and other material set out in the associated appendices should not be used for any other purpose: if they are so used, it is entirely at the risk of the user.

Dean

Faculty of Engineering

Certification of Dissertation

I certify that the ideas, designs and experimental work, results, analyses, and conclusions set out in this dissertation are entirely my own efforts, except where otherwise indicated and acknowledged.

I further certify that the work is original and has not been previously submitted for assessment in any other course or institution, except where specifically stated.

Matthew Trent

Student Number: ███████

Acknowledgements

I would like to express my gratitude to the individuals who have supported me throughout this research project.

My wife and parents who have stood by me and continued to encourage and support me throughout this academic journey.

Dr Andy Nguyen for his valuable guidance and academic support provided as my UniSQ project supervisor.

Dr Tony Le and Dr Sukhi Sendanayake for their contributions in providing additional guidance and support with the research and development of the numerical programs.

Matthew Trent

Table of Contents

List of Figures

List of Tables

Abbreviations

CAD   Computer Aided Drawing
FEA   Finite element analyses
GPa   Gigapascals
Hex   Hexahedral
IMC   Intermodular Connection
kN   Kilonewton
kNm   Kilonewton metre
MIC   Modular Integrated Construction
MPa   Megapascals
P-T   Post-tensioned
RP   Reference Point
v.   Version

Chapter 1   Introduction

1.1   Overview

Modular Integrated Construction (MIC) is an innovative construction system that utilises off-site prefabrication methods to create three-dimensional rectangular segments of a building in an established off-site production facility. These prefabricated modular segments are transported from the production facility to the construction site, where they are lifted into place by a crane and assembled to form a complete structure. The modules are typically constructed using steel frames for the structural framework because they can be easily fabricated off-site and then deployed on-site to develop modular structures.

One of the most effective forms of MIC technology involves corner-supported modular steel structures constructed from rectangular modules. However, despite the advantages of steel-framed modular buildings, their application is limited to low to medium-rise buildings, Shan & Pan, (2020). Modular steel buildings are made up of three-dimensional volumetric units and differ from conventional steel building systems that have continuous beam and column connections. Corner supported modular steel buildings are discontinuous in nature and rely on structurally sound connections, usually placed within the corners of the modules, to establish a continuous structural building system.

Due to the discontinuous placement of joints, high concentrations of stress develop in these sections of the modular building systems, and the IMCs (Intermodular Connections) are responsible for the distribution of forces, bending moments, and deformations. The key to the overall structural performance of modular integrated buildings, which distinguishes their design from traditional counterparts, lies in the impact of connections between the units, on the distribution of forces, moments, stability, and deformations of the frame. The stiffness, strength, and rotational capacity of interconnections are three structural characteristics that directly affect the performance of modular structures, (Farajian et al. 2022). IMCs are essential to the functioning of modular structures and bring the individual modules together to form a complete modular building. Therefore, the structural capacity of IMCs should be well defined to reliably transfer forces through the connections and throughout the building.

1.2   Problem Statement

Numerous IMC systems have been developed to improve the constructability and functionality of modular structures, each with their own benefits and limitations. A significant problem is creating and designing reliable connection systems with more research needed to better define their behaviours. A study by, (Lacey et al. 2019b), observed that rotational effects from various force transmissions led to gap development in a P-T (post-tensioned) IMC that creates inter-story drift and connection slip. Another research by (Lacey et al. 2020) on an interlocking IMC showed significant slippage between the two connections, resulting in undesirable shear effects to the shear pins and bolts. An improved connection that addresses the issues with the above connection systems can provide an effective solution for the building industry.

1.3   Project Aims and Objectives

The aim of this project is to develop a Novel IMC model based on the combination of two existing IMC models published by (Lacey et al. 2019b and 2020). The Novel IMC model will be analysed under a range of loading scenarios to review and verify the model's responses to specific loading applications.

The specific project objectives are:

- Develop the Replica A1 numerical model in Abaqus to calibrate and validate the numerical program against published experimental and numerical data and information.
- Develop the Replica P-T and 2C models in Abaqus based on the settings and parameters established in the validation program.
- Develop the Novel IMC model in Abaqus based on the two reference models.
- Run equivalent loading scenarios on the P-T, 2C and Novel IMC models and extract and graph the results.
- Identify and confirm the gap development and slippage problems existential in the post-tensioned and 2C models respectively.
- Review and compare the results from the numerical analysis on the Novel IMC model compared with the replica P-T and 2C IMC models.
- Identify the differences in slippage, gap development and any improvements or deterioration between the pre-existing IMC models and the Novel IMC model.

2

1.4   Scope and Limitations

The research was conducted using the numerical analysis program ABAQUS v.2019 to analyse the behaviour of two selected reference models, namely the P-T and 2C IMC models, as well as the proposed Novel IMC model. Various loading scenarios, including shear, axial, bending moments, and combined loading cases, were applied to the models. The reactions of each model to the applied loads were compared and assessed to determine the differences in behaviour under equivalent loading scenarios.

Due to limited time and funding, experimental testing was not completed on any of the models in this research project. Consequently, the ability to calibrate or validate the numerical Novel IMC model against actual experimental results is limited to settings established from published data related to a similar model. Additionally, the positions for restraints and loading in the numerical models were determined based on information extracted from reference papers, most notably (Lacey et al., 2020). Whereas the actual behaviour of IMCs is dependent on the transmission of forces through the columns. This differs from the approach of applying loads and restraints to confined geometric positions, such as between the connection and the ends of the columns. Furthermore, the loading scenarios applied to the models in this project were limited to incremental linear loads, in contrast to alternating dynamic loads, as seen in an earthquake scenario.

1.5   Dissertation outline

Chapter 1; Intermodular connections within modular buildings are introduced to emphasize their importance in distributing forces through the connections and throughout the building. The problem is defined, and the project's aims and objectives are established, followed by an outline of the scope and limitations of the research activities.

Chapter 2; Covers the literature review, outlining load transmission in modular buildings and the behaviour of the IMCs in modular structures. Different types of IMCs are reviewed, along with the systems of analysing their behaviour under load, and the need for an improved IMC is discussed.

Chapter 3; The research methodology, provides details on establishing the numerical program for the A1, P-T, 2C and Novel IMC models selected for this research project.

Chapter 4; Validation of intermodular connection modelling techniques involves establishing the A1 validation model and verifying the results by comparing them with published data from experimental and numerical results in (Lacey et al. 2019 a).

Chapter 5; Development of a Novel Intermodular Connection, provides specific steps to develop the Novel IMC model including the verification of the model behaviour and a parametric analysis.

Chapter 6; Results and discussion, outlines the loading scenarios applied to the models and discusses the behaviour of each model under the different loading cases.

Chapter 7; Concludes the dissertation providing a summary of the research findings, contributions, limitations, and opportunities for further research.

Chapter 2   Literature Review

2.1   Introduction

One of the most effective building technologies for the next generation of prefabricated building construction is modular steel structures constructed of volumetric custom prefabricated pieces. The key to the overall structural performance of these systems, which distinguishes their design from that of its traditional counterparts, is the impact of connections between the units, or 'interconnections', on the distribution of forces, moments, stability, and deformations of the frame. The stiffness, strength, and rotational capacity of interconnections are three structural characteristics that directly affect the performance of modular structures (Farajian et al. 2022).

2.2   Load transmission in modular building

Modular buildings structural behaviour is different to traditional structures, and the intermodular connections determine their operational performance. The key difference between traditional and modular buildings is the structural performance of intermodular connections that join the modules together. Modular buildings exhibit complex structural behaviours within the connections due to the discontinuous nature of these corner supported modular frame systems. High concentrations of stress develop within the intermodular connections due to the discontinuous transmission of forces. The inter modular connections are responsible for the transmission of important structural behaviours including, shear, axial, and moment-rotation. The ability of modular structures to sustain applied loads depends on the interconnection of frame members and modules. However, there is limited research on IMCs despite the need for a better understanding. Further research is needed to facilitate the design of modular buildings and IMCs to better comprehend these structures, (Lacey 2020).

2.3 Intermodular Connection Design

A review by (Nadeem et al. 2021), provides a thorough explanation of the key aspects of intermodular connections, including geometric designs, structural performances, and contemporary design methodologies. Using earlier accessible experimental and theoretical investigations, the advantages and disadvantages of the current configurations are examined in terms of the structural performances.

Several types of intermodular connections have been developed, each with their advantages and drawbacks. Some of the connection types include self-lock connections, vector block connections, vertical post-tensioned connections, in-situ bolted-welded joints, in-situ bolted beam-to-column connections, bolted connections with welded cover plates, and semi-rigid bolted plate-type connections (Nadeem et al. 2021).
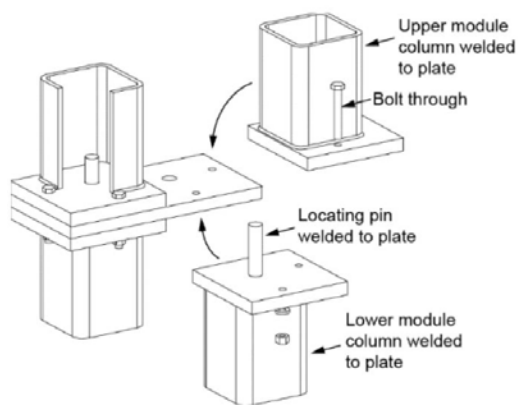
Figure 1.1: Bolted IMC Lacey et al. (2020)
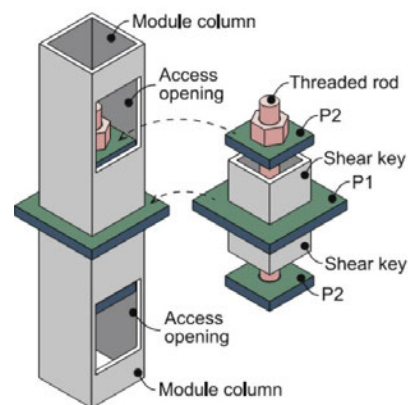
Figure 1.2: Post-tensioned IMC, Lacey et al. (2019 b)
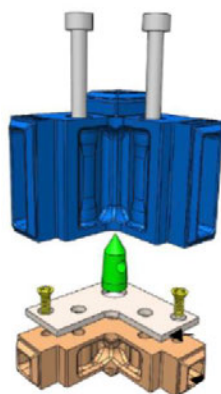
Figure 1.3: Vector block IMC, Dhanapal et al. (2019)
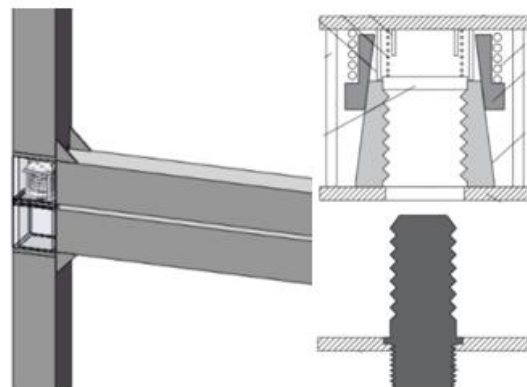
Figure 1.4: Self lock IMC, Dai et al. (2019)

The construction of modular buildings depends on how quickly and easily the modules can be joined, and the constructability of the modular structure is significantly affected by the IMCs geometry. The development of an efficient, simple, and effective connection has proven to be a challenging task. For example, bolted connections are easy to install, but due to hole tolerances, they can lead to the early development of sliding between the connections. Post-tensioned connections offer reasonable support against axial and shear forces; however, they develop gaps between the connections when the capacity of the P-T rod is exceeded. On the other hand, welded connections entail more on-site work and cannot be easily disassembled compared to bolted or post-tensioned connections. The design and geometric characteristics of intermodular connections have been observed to significantly impact the behaviour of both the IMC and the modular structure as a whole. Welded and bolt-type connections provide improved behavioural characteristics, although they require more workspace and effort to install compared to plug-in-type connections, which can be quickly and easily installed, with the trade-off being decreased structural capacity (Nadeem et al. 2021).

2.4   Intermodular Connection behaviour

(Lacey, Chen & Hao 2022) reviewed the most recent experimental systems used for analysing IMCs in modular structures. Three systems of investigation are established for the structural response: joint (J), frame (F) and module (M). Further categorisation of the joints is defined as: beam loading (J/B), stub column assembly (J/S), column loading (J/C) and beam-column (BC). Unbraced frames are susceptible to failure in the welded beam to column connection before IMC behaviour is noticeable and are better suited to the J/C test. Whereas the J/S test is more suited for use with braced frames. The response to quasi-static uniaxial monotonic and cyclic lateral stresses is the focus of the currently available experimental investigations. It is still necessary to develop experimental techniques for biaxial lateral and dynamic activities. IMC behaviour is greatly influenced by geometric and design features. Constraints in bolted and welded IMCs are increased by the workspace. To overcome these restrictions alternative plug-in systems are suggested, although this increases geometric complexities and reveals an ambiguous path for load transfer. Additionally, (Nadeem et al. 2021) reveals that, IMCs are found to have more complex load mechanisms than conventional steel connections. And due to the floor and ceiling beams acting differently, the load mechanisms have greater complexities and cannot effectively be modelled through conventional simulations. (Farajian

et al. 2022) mentions, the effect of the connections or 'inter-connections' on the distribution of moments, forces and stability between the modules is the key to the overall structural performance and distinguishes the design from traditional steel frame buildings. The stiffness, strength, and rotational capacity of interconnections are three structural characteristics that directly affect the performance of modular structures. Three performance criteria are considered by (Farajian et al. 2022), to categorise interconnections in sway corner-supported modular frames for rotational stiffness and strength characteristics. (I) Buckling criteria is based on the ultimate limit state, (ii) displacement/drift criterion is based on the serviceability limit state, and (iii) combined buckling and displacement/drift criterion based on the ultimate limit state. Also, depending on the ultimate moment capacity of interconnections, interconnections are divided into three categories: fully-strength, partial-strength, and nominally pinned. This categorisation system can be implemented in the first stages of design to select appropriate design process and approach for each category.

2.5   Analyses and Testing of Intermodular Connections

Effectively analysing and designing intermodular connections requires both experimental testing and numerical simulation. Physical experimentation can be completed with the production of prototypes placed under various loading scenarios to replicate forces transmitted through the joints, revealing the model's reaction and behaviour with respect to applied loading scenarios. On the other hand, finite element analysis software such as ANSYS or ABAQUS can be utilised to conduct numerical simulations. Digital models that replicate the connection's geometry, material properties and boundary conditions are developed and processed through the software. The simulation provides a virtual representation of the protypes behaviour under given loading scenarios.

2.6   Experimental testing of Intermodular Connections

Experimental testing was conducted on IMCs in the study titled 'Seismic Mitigation of Steel Modular Buildings Using Novel Inter-Modular Connections' by (Sukhi 2020). The investigations followed initial numerical analyses to provide more accurate results on the strength and feasibility of the IMCs studied. The geometry matched the numerical model to

that of a half symmetrical model to simulate the behaviour of four adjacent modules, with the column's lengths set to 0.5 m. A test specimen was arranged horizontally, with one end fixed, while the other end was connected to an actuator via a hinge. The actuator was powered by a 500 kN hydraulic ram to apply both monotonic and cyclic loads to the test specimen. Complex instrumentation was used in the experimental set up to capture the response of the test specimen under loading including, Strain Gauges, Linear Variable Displacement Transducers and Laser Displacement Sensors. Monotonic testing was conducted against four different configurations of the test specimen until they failed due to yielding and or plastic deformation. Cyclic load testing was also conducted on the same configuration of test specimens, with the loading cycle continuing until weld failure was observed or a decrease of moment capacity was noticed (Sukhi 2020). The experimental testing provided a comprehensive range of results of the specimens' behaviour under the given loading scenarios.

An experimental setup was conducted in a study titled 'New Interlocking Inter-Module Connection for Modular Steel Buildings: Experimental and Numerical Studies' by (Lacey et al. 2019a). The experiment involved a half-symmetrical model designed to simulate the shear behaviour between four adjacent modules, with the column lengths set at 50 and 75 mm. Six specimens were established, with three variations, including two specimens with different bolt hole geometries, and another excluding the shear pin. The experimental models were set up under a press, and a bearing force of up to 250 kN was applied to the upper columns, while they were supported by a bearing under the adjacent lower columns. This loading configuration created a shear force between the adjacent plates to reveal the slip behaviour under shear loading scenarios. As a result, the displacement was graphed in comparison to the applied shear force, illustrating the slip behaviour of the model under this loading scenario in a physical context.

An experimental analysis by (Rajanayagam et al. 2022) was conducted to investigate the shear behaviour of an IMC under lateral loading. The specimen included four columns to replicate a half-symmetrical model, based on the grouping of eight adjacent modules. The specimen was placed under a press with a loading capacity of 500 kN, with one side of the plates supported underneath by a bearing, and the load applied to the other side to generate the shear force between the plates. The strain was captured using an advanced photogrammetry system that calculates strain through a contactless measurement system. Therefore, the displacement and

load values were captured and graphed to illustrate the relationship between force and slip behaviour.

2.7   Numerical Analyses of Intermodular Connections

The numerical analysis program ABAQUS v.16.4.2 was implemented to investigate the behaviour of IMCs in modular buildings in the study titled "Seismic Mitigation of Steel Modular Buildings Using Novel Inter-Modular Connections" by (Sukhi 2020). ' Half-symmetrical models were developed to simulate eight adjacent modules, reducing computational demand. The columns were modelled in 0.5 m lengths, in contrast to the standard 3 m lengths typically found in modular units. The selected meshing approach utilized first-order 8-node linear brick elements. Smaller elements were employed to model the bolts, enhancing contact accuracy. The interaction between parts was defined using a penalty friction model, with different coefficients appropriately assigned to different materials. Material properties were established using a bi-linear profile, with the modulus of elasticity set at 200 GPa and Poisson's ratio at 0.3 for all steel parts. Finally, a replica numerical model was validated against published numerical and experimental results by (Gunawardana et al. 2016), which showed similar behaviour to that of the established model (Sukhi 2020).

A study titled 'New Interlocking Inter-Module Connection for Modular Steel Buildings: Experimental and Numerical Studies' by (Lacey et al. 2019a) implemented the FEA program ABAQUS V.6.14 to complete numerical analysis on the selected models. The model was established as a quarter-symmetrical model based on the experimental specimen. Symmetry boundary conditions are applied to the faces where the model is dissected from the full model. The friction coefficient between the plates is set to 0.3146, and the elastic slip is set at 0.001 mm, with hard normal contact and separation allowed for normal behaviour. The coefficient of friction between the bolt head and plates was taken as 0.05 and between the bolt shank and plates was taken as frictionless. The mesh was established with first order 8 mode linear brick elements and a sensitivity analysis with mesh sizes of 1, 2, 3 and 4 mm were conducted. The nominal mesh size of 2 mm was adopted finding little difference compared to the results obtained from the 1 mm mesh size. The numerical model was calibrated against the results provided by the experimental analyses. However, the displacement vs. force curves did not follow the same path. This discrepancy was attributed to the variation in the friction interface of the experimental model compared to the constant friction interface in the numerical model.

(Rajanayagam et al. 2022), conducted a numerical analysis to assess the behaviour of a selected IMC type under lateral loading, simulating shear behaviour between the plates. The FEA program ANSYS was selected to complete the numerical analyses on these models, and the numerical program was validated against the experimental displacement versus force results. The meshing consisted of 'Solid 185' with elasto-plastic stress-strain behaviour to model the steel material. A mesh size of 1.0 mm was selected to control the length to width aspect ratios. The modulus of elasticity was taken as 200 GPa, and the shear modulus to 80 GPa. The yield strengths for the SHS and plates were both specified as 350 MPa.

2.8   Intermodular Connection testing systems

Finite element analyses and mechanical testing can be implemented to categorise the mechanical properties of both inter- and intra-connections. Both methods were utilised by Farajian et al. (2022) to determine the properties of the two types of connections. Farajian et al. (2022) used these methodologies for developing a system to model, analyse and create horizontal and vertical interconnections in a modular frame with sway corners.

Utilising theoretical, experimental, and numerical analyses (Rajanayagam et al. 2022) completes a thorough investigation of the inter-modular connection shear behaviour under lateral stress. Three design configurations of the selected inter-modular connection were tested in shear with various bolt sizes and hole tolerances, and their load-deformation behaviours were investigated. Then, in ANSYS, finite element models were created and verified using test findings from the trials. Since the connections frequently break in slippage even under extremely light lateral loads, they were classified as slip critical connections for serviceability design. Additionally, analysis of combined tension and shear effects on the connections revealed that the failures were caused by the combined effect and not only by shear (Rajanayagam et al. 2022).

More experimental evaluation is required to assess the influencing parameters, including the intermodular connection arrangement, the existence of ceiling beams, the eccentricity at connections, and the degree of stiffness. Also, alternative plug-in systems can be utilised to mitigate in-situ welding needs and avoid workspace requirements. And for accurate numerical

modelling and simulations of IMCs, analytical models are needed to calculate the parameters for strength, stiffness, and deformation. Load path transfer mechanisms are still unclear and require more investigations and analyses. What is more, further research is needed to determine the behaviour and characteristics of IMCs under complicated loading situations including, blast, earthquake and wind loads (Nadeem et al. 2021).

2.9   Intermodular Connection knowledge gap

To better understand the structural behaviour of inter-module connections and to create suitable theoretical model analyses, more research is required on the structural behaviour of intermodular connections. Additionally, it is necessary to develop appropriate experimental techniques and consider combined actions, as suggested by (Lacey et al. 2019). Furthermore, further investigation into the causes of slip between joints should be conducted. By gaining a better understanding of the causes and effects of slip between joints, mitigating systems can be developed to address these issues. Further research into the effects of gap openings between columns and beams can be completed. These cumulative effects of gap openings contribute to inter-story drift for tall buildings. The development of numerical models to replicate the stiffness, strength, stress distribution, and energy dissipation for selected connection types can simulate the behaviour of modular steel buildings in different scenarios.

Intermodular connections in modular steel buildings are critical components required to connect individual module units to form a multi-level building. These intermodular connections play an intrinsic role in the overall performance of modular steel buildings because they are responsible for transferring forces, moments, and deformations of the frame through to the foundation. Despite their importance, it appears that designing a reliable intermodular connection remains a significant challenge in modular steel building design. This research will address the issue of IMC design by developing a Novel IMC model that combines two existing IMC models with the objective of enhancing IMC performance under expected loading scenarios.

Chapter 3   Methodology

3.1   Introduction

Numerical analysis was selected to investigate the behaviour of the IMC models under various loading scenarios, as it offers a more efficient and cost-effective alternative to experimental analyses. In the study conducted by (Lacey et al. 2019 & 2020), the FEA software ABAQUS v.6.14 was employed to analyse the behaviour of both the 2C and A1 models, which serve as integral references for this research project. Therefore, ABAQUS v.2019 was selected for replicating and developing the A1 validation model, the 2C and P-T reference models, and the Novel IMC model.

There are four IMC models that were required to be developed in this investigation. First, the A1 replica model was established to calibrate and validate the numerical program against experimental and numerical results provided in (Lacey et al. 2019a). Next the 2C and P-T replica models are established based on the information provided in Lacey et al. (2019a & 2020). Finally, the Novel IMC model is developed based on the combination of the 2C and P-T models.

Figure 3-2.1: Numerical Analyses Methodology Flow Chart

Develop Numerical Models Using Abaqus		
A1 Replica	2C Replica	P-T Replica

Establish Geometry		
Assign Material Properties	Partition parts	Assemble model

Establish Interactions		
Interaction Properties	Boundary Conditions	Loading Conditions

Mesh the Model

Establish Analyses Parameters		
Step settings	History output	Solver settings

Run the Analyses		
Extract Data	Graph the data	Review the results

3.2   Geometry

Geometry can be developed directly in Abaqus or imported from CAD programs such as AutoCAD and SolidWorks. The development of the IMC models for this research were completed directly in ABAQUS as it was found to give greater user control with editing parts during construction of the model.

3.2.1   A1 IMC Replica

The A1 interlocking model is a one-quarter symmetrical model replicated from (Lacey et al. 2019a). While dimensions and positions were provided for all parts, the specific position of the shear pin and the size of the bolt and nut were not clear. The shear pin's position was determined through proportional measurements in Revu Bluebeam, while the dimensions of the bolt head and nuts were established using a combination of proportional measurements and specifications provided by (United Fasteners Australia 2023).

3.2.2   2C IMC Replica

The 2C replica model was developed from the information provided by (Lacey et al. 2020). The dimensions and positions were provided for all the parts, however as above it was not clear the exact positions of the shear pin and size of the bolt head and nut. The position of the pin and dimensions of the bolt head and nut were determined as mentioned above.

3.2.3   P-T IMC Replica

The P-T IMC model was replicated from the information provided in (Lacey et al. 2019b). The dimensions and positions were provided for all the parts although the bolt nut was not clearly defined. This was determined by proportional measurement from the reference text and specifications provided by (United Fasteners Australia 2023).

3.2.4   Novel IMC

The Novel IMC model is based on the combination of both the 2C and P-T models. The development of this model is discussed further in Chapter 5 Development of a Novel-Intermodular Connection.

3.3   Partitions

Partitions were used to divide the individual parts of the model into simpler shapes to improve meshing. This allows for complex geometry to be broken down into more manageable shapes and produces more efficient and accurate meshing. The partitions allowed for segregation between different contact and interactions to accurately define contact surfaces where there are multiple interactions on the same surface pairs. This also allows for the accurate application of boundary conditions for specified areas. Furthermore, partitions between the adjacent parts in each model were kept inline to improve processing of the numerical model.

3.4   Material Properties

The material properties are based on Lacey et al. (2019 b and 2020) with the Modulus of Elasticity as 200 GPa and Poisons ratio at 0.25. However, exception was given to the stress strain curve implementing a bi-linear profile compared to a quad-linear profile. The behavioural characteristics were briefly examined, showing little difference by implementation of either quad or bi linear stress strain curves. See Appendix B for material properties calculations.

Description	Min yield stress (MPa)	Min tensile strength (MPa)	Min elongation (%)
SHS Column, AS/NZS 1163	350	430	12
Plate, AS/NZS 3678	360	450	20
R12 Locating pin	375	530	32
M12x1.75Px50,8.8,HR Bolts AS/NZS 1252	640	800	12
Sampson M20 threaded rod Class 8.8	660	800	12

Table 2-1: Material Properties, Adapted from: Lacey et al. (2020)

3.5   Interaction Properties

The interaction parameters are set as hard normal contact with separation allowed for all surface interactions and elastic slip set at 0.001. The coefficient of friction for surface-to-surface interactions are established as 0.3146 for the plate to plate, 0.3 for column to column, 0.2 for locating pin to plate, 0.075 for bolt to plate at all instances, and frictionless between the post tensioned rod nut and cap plate respectively.

Interaction Properties			
Interaction pair		Friction	Elastic Slip
Plate	Plate	0.3146	0.001
Column	Column	0.3	0.001
Plate	Locating pin	0.2	0.001
Plate	Bolt head	0.075	0.001
Plate	Bolt shank	0.075	0.001

Table 2-2: Interaction Properties, Adapted from: Lacey et al. (2020)

3.5   Loading and Boundary Conditions

The loading and boundary conditions have been established to maintain equivalent behaviour between the three models. For the application of the restraint all three models implement a fixed restraint on top of the lower column between the column and the plate as pictured in figures 3.13, 3.14, 3.15. For application of the shear force the load was applied to the bottom of the upper column webs as pictured in figures 3.16, 3.17, 3.18. The axial loads were similarly applied to the top of the upper columns. For each of the models there was some difference to the height at the top of the upper column where 2C is 50 mm, post tensioned replica is 69 mm and the novel IMC is 100 mm from plate to top of upper column respectively. The application of bending moments is also applied to the top of the upper columns on the same positions as the axial loads.

3.6   Meshing
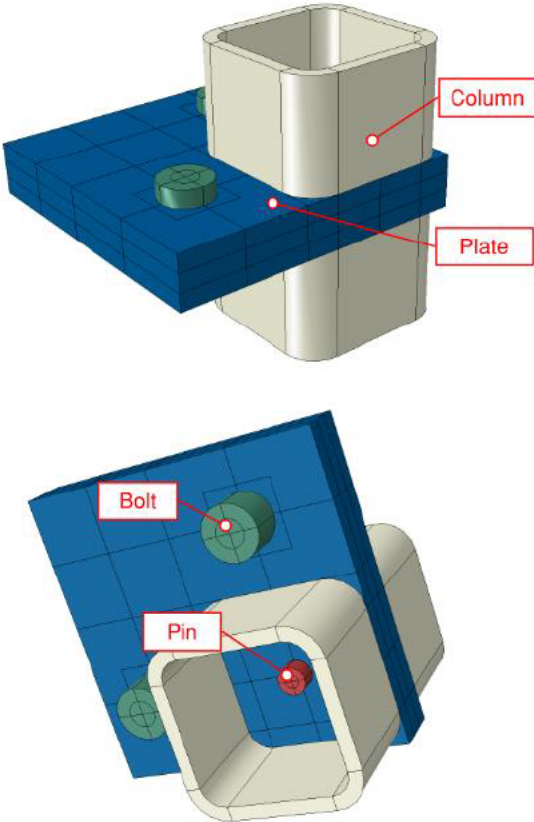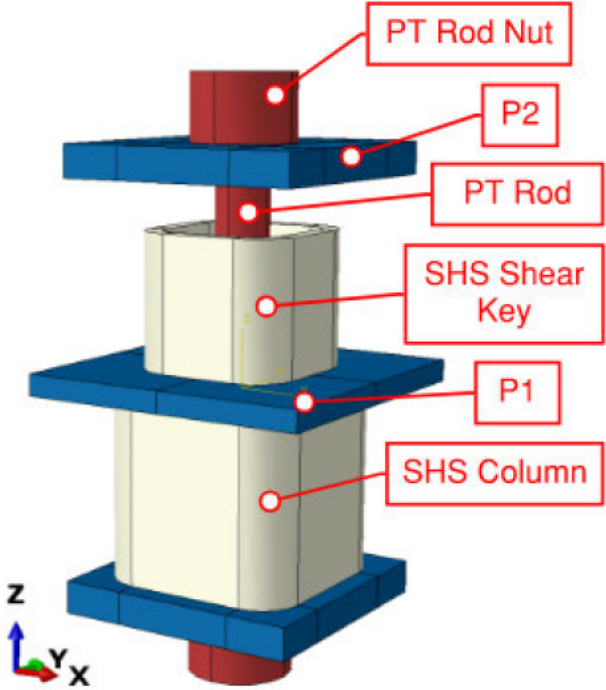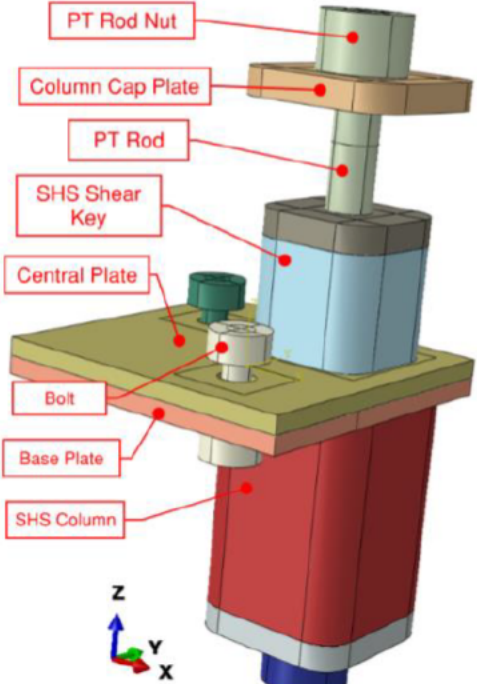
The meshing has been selected as 4 mm mesh size of first order 8 node linear brick elements. Hex (hexahedral) shape elements were selected due to their reduced computational cost compared to tetrahedral and wedge type elements. Bolts and pins are meshed using a wedge-style arrangement with a 2 mm sizing to create a finer mesh pattern that is better suited to their nonlinear geometry.

3.7   Mesh sensitivity studies.

Mesh sensitivity studies are conducted using the replica A1 validation model to determine the optimal mesh size. These studies follow the successful establishment and completion of the A1 numerical model. Analyses with mesh sizes of 2, 3, 4, and 6 mm will be performed to identify the mesh size that offers accurate results and balanced computational efficiency.

3.8 Model Geometry and Property Comparison

Table 2-3: 2C, P-T and Novel IMC Model Geometry and Properties

2C Replica	P-T Replica	Novel IMC
Figure 2.2: 2C Replica IMC model	Figure 2.3: P-T Replica IMC model	Figure 2.4: Novel IMC model

Column and Plate Section
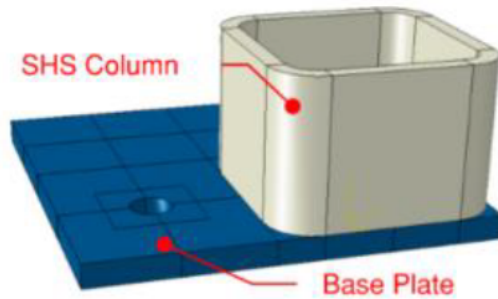
Figure 2.5: 2C Replica base plate and column
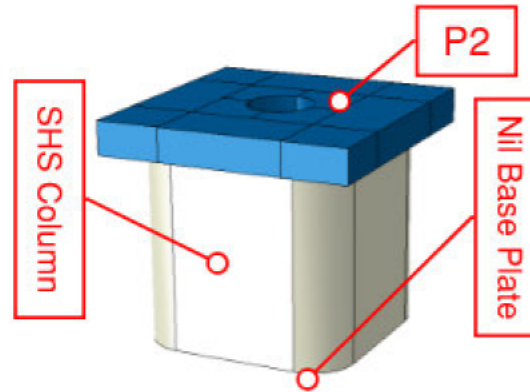
Figure 2.6: P-T Replica column and upper plate
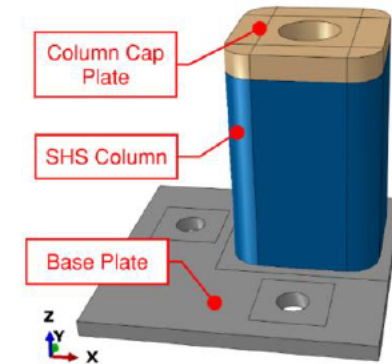
Figure 2.7 Novel IMC base plate, column & cap plate

SHS Column

Geometry (mm)				Geometry (mm)				Geometry (mm)			
Length/Height	Width	Depth	Wall	Length/Height	Width	Depth	Wall	Length/Height	Width	Depth	Wall
50	75	75	6.0	69	75	75	6.0	100	75	75	6.0
Material Properties				Material Properties				Material Properties			
	Yield stress (MPa)	Plastic strain (%)			Yield stress (MPa)	Plastic strain (%)			Yield stress (MPa)	Plastic strain (%)	
f_y 1	350	0.0		f_y 1	350	0.0		f_y 1	350	0.0	
f_y 2	430	0.118		f_y 2	430	0.118		f_y 2	430	0.118	

Base Plate							
Geometry (mm)					Geometry (mm)		
Length/Height	Width	Depth	Nil		Length/Height	Width	Depth
8.0	135	135			8.0	141	141
Material Properties					Material Properties		
	Yield stress (MPa)	Plastic strain (%)				Yield stress (MPa)	Plastic strain (%)
f_y 1	360	0.0			f_y 1	360	0.0
f_y 2	450	0.198			f_y 2	450	0.198
			P2		Column Cap Plate		
			Geometry (mm)		Geometry (mm)		
			Width	Depth	Depth	Length/Height	Depth	Depth
			12.0	91.0	91.0	12	75	75
			Material Properties			Material Properties		
				Yield stress	Plastic strain		Yield stress (MPa)	Plastic strain (%)
			f_y 1	360	0.0	f_y 1	360	0.0
			f_y 2	450	0.198	f_y 2	450	0.198

IMC Shear Key and Plate Section
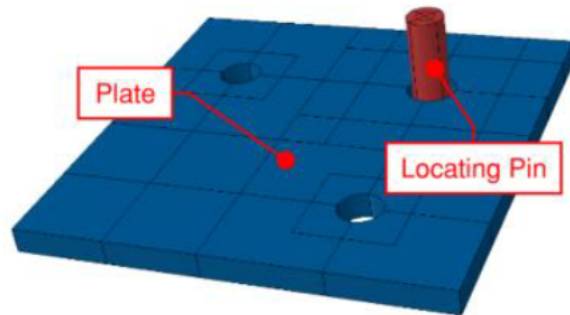
Figure 2.8: 2C Replica central plate and pin
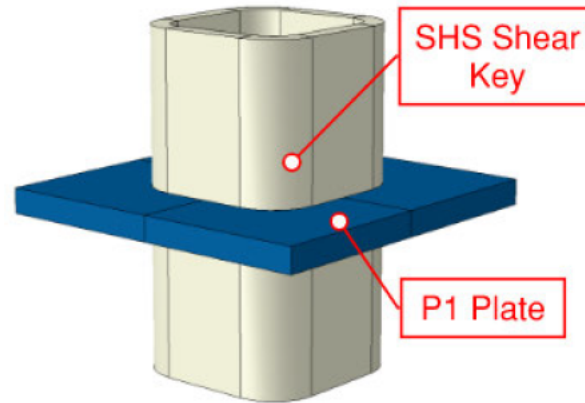
Figure 2.9: P-T Replica central plate and shear keys
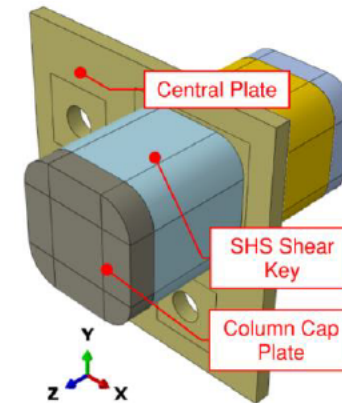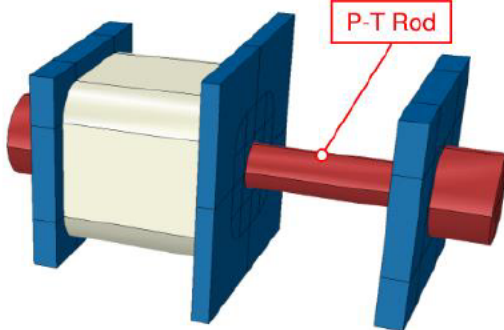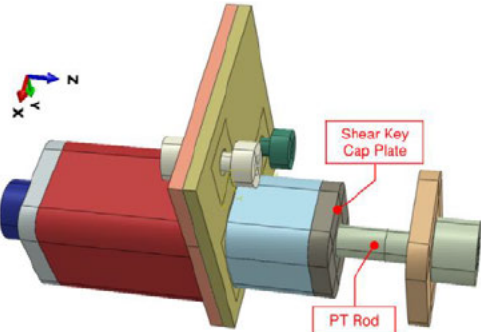
Figure 2.10: Novel IMC central plate, shear keys & cap plates
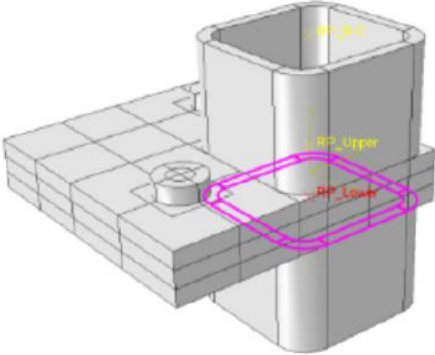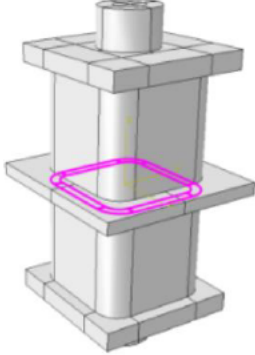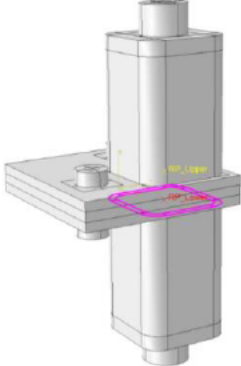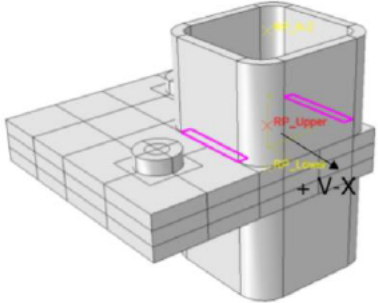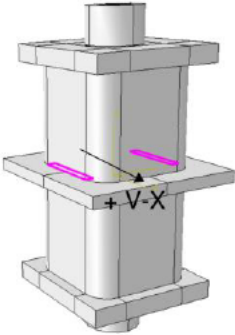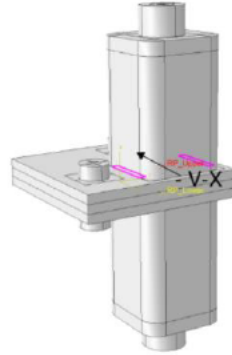
SHS Shear Key								
Nil	Geometry (mm)				Geometry (mm)			
	Length/Height	Width	Depth	Wall (T)	Length/Height	Width	Depth	Wall (T)
	50.0	59.0	59.0	6.0	50.0	59.0	59.0	6.0
	Material Properties				Material Properties			
		Yield stress (MPa)	Plastic strain (%)			Yield stress (MPa)	Plastic strain (%)	
	f_y 1	350	0.0		f_y 1	350	0.0	
	f_y 2	430	0.118		f_y 2	430	0.118	

Central Plate								
Geometry (mm)			Geometry (mm)			Geometry (mm)		
Length/Height	Width	Depth	Length/Height	Width	Depth	Length/Height	Width	Depth
8.0	135	135	8.0	109	109	8.0	141.0	141.0
Material Properties			Material Properties			Material Properties		
	Yield stress (MPa)	Plastic strain (%)		Yield stress (MPa)	Plastic strain (%)		Yield stress (MPa)	Plastic strain (%)
f_y 1	360	0.0	f_y 1	360	0.0	f_y 1	360	0.0
f_y 2	450	0.198	f_y 2	450	0.198	f_y 2	450	0.198

Locating Pin				Shear Key Cap Plate		
Geometry (mm)				Geometry (mm)		
Length		Diameter		Length/Height	Width	Depth
-		12		12.0	59.0	59.0
Material Properties				Material Properties		
	Yield stress (MPa)	Plastic strain (%)			Yield stress (MPa)	Plastic strain (%)
f_y 1	375	0.0		f_y 1	360	0.0
f_y 2	530	0.318		f_y 2	450	0.198

IMC Post Tensioned Rod		
	Figure 2.11: P-T Replica post-tensioned rod view	Figure 2.12: Novel IMC post-tensioned rod view
	Threaded Rod	Post Tensioned Rod

	Geometry (mm)			Geometry (mm)		
	Length		Diameter	Length		Diameter
	-		20	-		20
	Material Properties			Material Properties		
		Yield stress (MPa)	Plastic strain (%)		Yield stress (MPa)	Plastic strain (%)
	f_y 1	660	0.0	f_y 1	520	0.0
	f_y 2	800	0.117	f_y 2	660	0.187

3.9   Model restraint and loading geometry

Table 2-4: Restraint and Load geometry

2C Replica	P-T Replica	Novel IMC
Restraint		
Figure 2.13: 2C Replica Restraint geometry	Figure 2.14: P-T Replica Restraint geometry	Figure 2.15: Novel IMC Restraint geometry
Shear loading Position and direction		
Figure 2.16: 2C Replica Positive Shear force load allocation	Figure 2.17: P-T Positive Shear force load allocation	Figure 2.18 Novel IMC neg Shear force load allocation

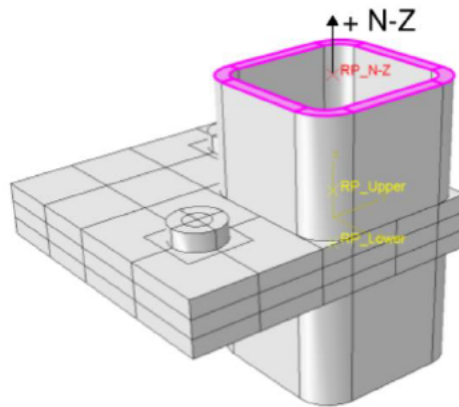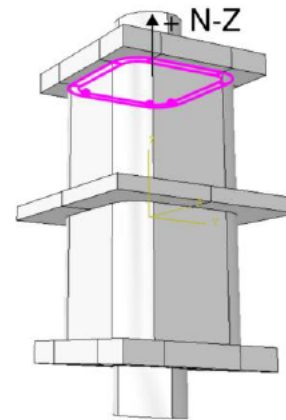| Axial loading Position and direction		
Figure 2.19: 2C Replica axial force loading allocation	Figure 2.20: P-T Replica axial force loading allocation	Figure 2.21: Novel IMC axial force loading allocation
Bending moment Position and Positive direction		
Figure 2.22: 2C Replica bending moment loading allocation	Figure 2.23: P-T Replica bending moment loading allocation	Figure 2.24: Novel IMC bending moment loading allocation
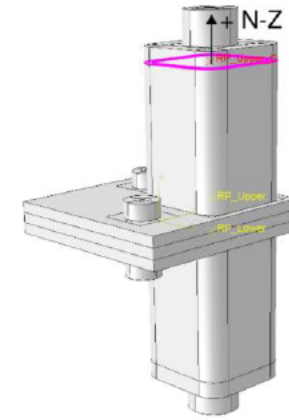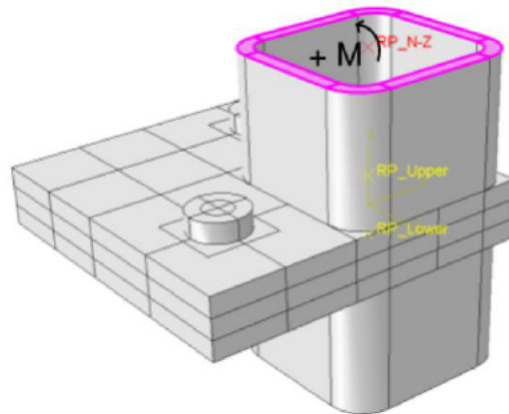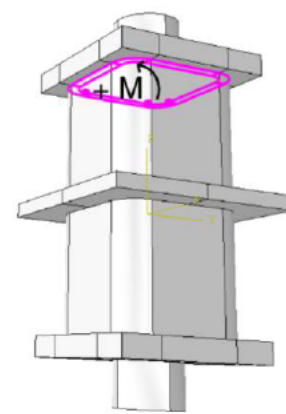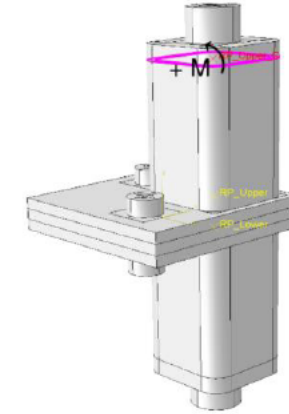
Chapter 4. Validation of Inter-Modular Connection Modelling Techniques

4.1   Overview

To validate and calibrate the numerical program, a model published in (Lacey et al. 2019a), listed as the A1 specimen, was replicated in the selected FEA program ABAQUS. Experimental and numerical testing were conducted on the A1 specimen under a shear loading scenario. The results of both the experimental and numerical analyses were published, demonstrating the slip vs. force behaviour under the specified loading conditions.

The A1 model was subsequently developed in ABAQUS based on the information found in the above-mentioned paper, with all of the model details and program parameters matched to the provided information. Including the quarter symmetrical establishment of the numerical model's geometry, as well as the incorporation of matching material properties, interaction properties and boundary conditions. Despite taking due care to match the replica A1 numerical model with the published A1 numerical and experimental models there were some discrepancies between the results. The replica numerical model developed slip at approximately 80 kN compared to the reference model that showed slip development at approximately 100 kN. Further validation studies were conducted on the 2C replica model with the 2C model published by (Lacey et al. 2020). The results between replica 2C and the published 2C numerical models showed a consistent trend in the numerical models' behaviour. Therefore, the replica numerical models have been verified as lower-bound numerical models.

Figure 3.1: A1 IMC experimental set up and A1 IMC section. Adapted from (Lacey et al. 2019 a)
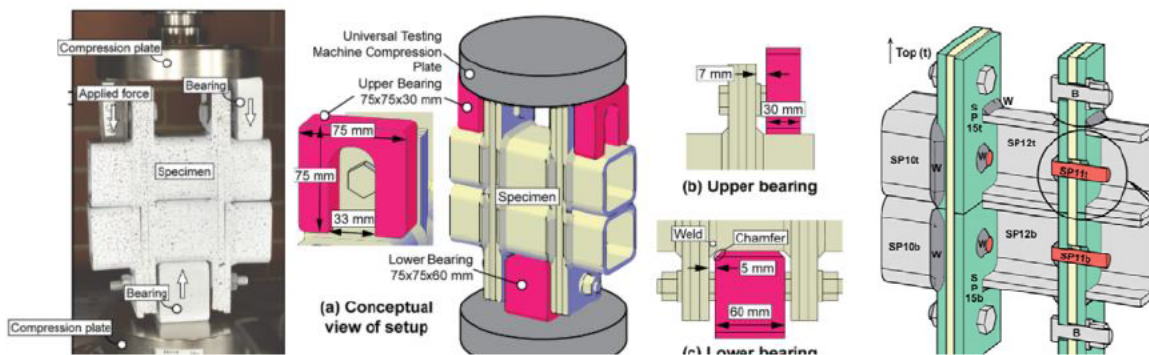
4.2 Development of model parts

The initial development of model parts was completed in AutoCAD and then imported into Abaqus as ACIS files. However, despite the initial advantage of creating 3D model parts in AutoCAD, there are limitations when it comes to making further modifications to the parts and models during the production of the numerical FEA model. Therefore, it was found that constructing the model components within the 'Create Parts' instance of ABAQUS was the most advantageous approach. This allows the modification and adjustment of parts to accommodate changes, such as altering the part's height, adjusting dimensions, adding partitions, and more.

4.3 Geometry

The geometry of the A1 model is based on the information provided in (Lacey et al. 2019a), with all part dimensions and positions matched to replicate the provided information. The geometry and layout of the parts are defined in table 4-1.

Table 3-1: A1 model geometrical identities

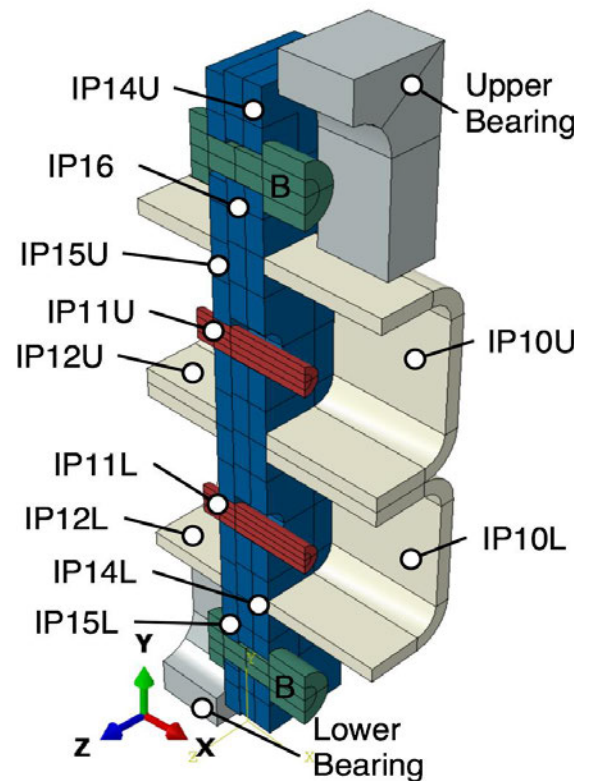| A1 symmetrical model Geometry				
Description/Part	Length (mm)	Width (mm)	Depth (mm)	Wall (T) (mm)
IP10 - Column	75	37.5	50	6.0
IP12 - Column	75	37.5	35	6.0
IP14 - Plate	135	37.5	8.0	NA
IP15 - Plate	135	37.5	8.0	NA
IP16 – Plate	135	37.5	8.0	NA
IP11 - Pin	12	12	50	NA
B - M12 Bolt	12	6	24	NA

Figure 3.2: A1 replica model

4.4   Material Properties

The material properties are equivalent for the 2C and A1 models, as specified in Chapter 3 Material Properties. Additionally, the transformation calculations for the plastic strain values are provided in Appendix B.

4.5   Interaction Properties

Due to the symmetrical layout of the A1 model, interaction settings are particularly important and require careful consideration, as they can influence the response of other settings. It was observed that improper surface interaction was a major cause of errors in the post-processing stage. Individually assigning interaction surfaces has been found to eliminate errors caused by improper allocation.

The assignment of loads and boundary conditions was transferred by reference points (RPs) to the allocated surface regions of interest. However, constraint types were found to have a significant impact on the behaviour of the numerical model during processing. Rigid body constraints were initially assigned between RPs and surface regions to establish connections. However, the numerical models were exiting the processing stage with errors before completion. An investigation found that coupling constraint types are recommended for models with dynamic behaviour under load. The implementation of coupling constraints allowed the numerical model to successfully complete post processing and this was a significant achievement.

Surface to surface interaction properties were matched with the reference model in all cases except for the bolt to plate friction coefficient. Where investigation revealed that the bolt to plate friction coefficient was not definitively defined. Lacey et al. (2019a) referred to Liu et al. (2017), who stated a friction coefficient of 0.05 for the bolt-to-plate interface and assumed frictionless between the bolt shank and the plates, without providing a citation or supporting experimental results. Further investigation found that bolt to plate friction coefficient varies in the range of $0.01 < x < 0.26$ Liu et al. (2020). Therefore, the bolt to plate friction coefficient was adjusted slightly from 0.05 to 0.075 for calibration of the numerical model to match the experimental results. All other interaction pairs are coincident with the 2C model and are listed in Chapter 3 Table 3-2.

4.6 Boundary conditions

Symmetry boundary conditions are applied to the faces where the model is dissected from the full model. Such that an X-symmetry is applied to the face in line with X-direction and Z-symmetry is applied to the face in line with Z-direction. Also, Y-antisymmetry is applied to the upper face of the upper bearing to replicate the behaviour of the bearing under loading from the press where movement is restricted to Y-direction only. The lower face of the lower bearing is fixed to restrict movement in all directions.
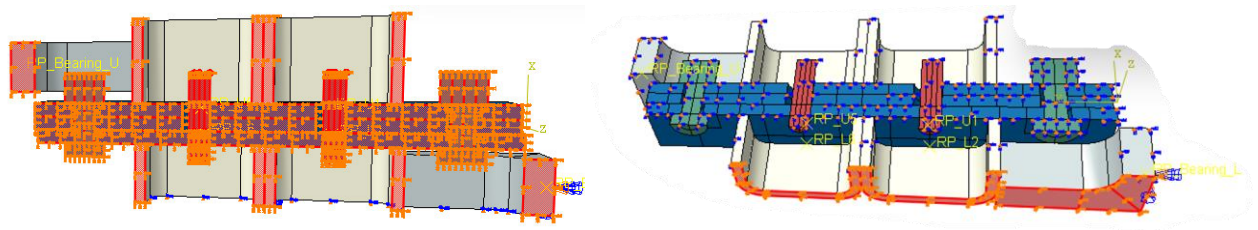
Figure 3.3: A1 Replica Symmetrical Boundary Conditions

4.7 Loading

The bolts were first pre-loaded to the required magnitude, followed by the application of a concentrated force to the upper bearing situated above the IP10U column. The upper bearing transferred the load into the IP10U column, replicating the slipping behaviour between the plates once the resistance to friction between the plates was exceeded.

4.8 Meshing

The mesh is selected as first-order 8-node linear brick elements with an average size of 4 mm. The 4 mm mesh size provides a good initial aspect ratio, ensuring that the mesh is proportionally divided into elements with a mesh-to-length ratio of less than or equal to 2:1. The 4 mm mesh size is examined for suitable accuracy under parametric analyse in a mesh sensitivity study.
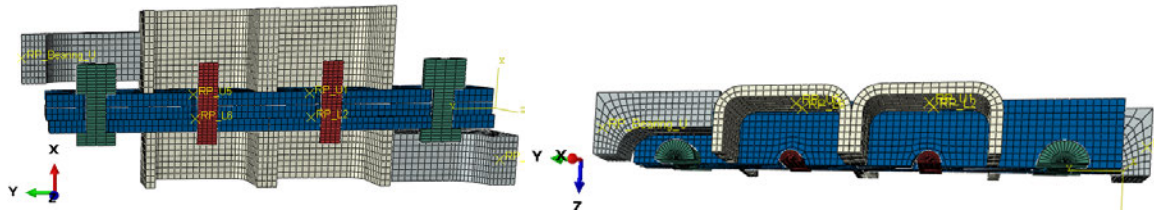
Figure 3.4: A1 Replica Mesh Layout

4.9 Step setting

The initial attempts to perform numerical analyses were completed with the step setting selected as 'static general.' However, due to the model being developed in a short timeframe, there were inherent modelling imperfections, and the model had difficulty converging under the 'static general' step setting. This issue was overcome by selecting the 'dynamic implicit' step setting, which is more tolerant of the modelling imperfections and nonlinearities found in these models. The implementation of 'dynamic implicit' marked a significant milestone in establishing the numerical model settings for the successful numerical processing of the FEA models in ABAQUS.

4.10   Results

The initial replica A1 model showed less resistance to slip against force, with slip initiating at approximately 75kN of applied bearing force. In comparison, the numerical A1 model developed by Lacey showed slip development occurring at approximately 100kN. To calibrate the replica A1 model the friction coefficient between the bolt and plates was adjusted to 0.075 from frictionless and 0.05 as established in, Lacey et al. (2019a). By increasing the coefficient from 0.05 to 0.075 the slip resistance increased slightly to initiate slip at approximately 80kN of applied bearing load. Therefore, the replica A1 model was successfully calibrated against the experimental data provided in (Lacey et al. 2019 a), such that the numerical model settings are validated to provide comparable results for modelling of the IMC models.
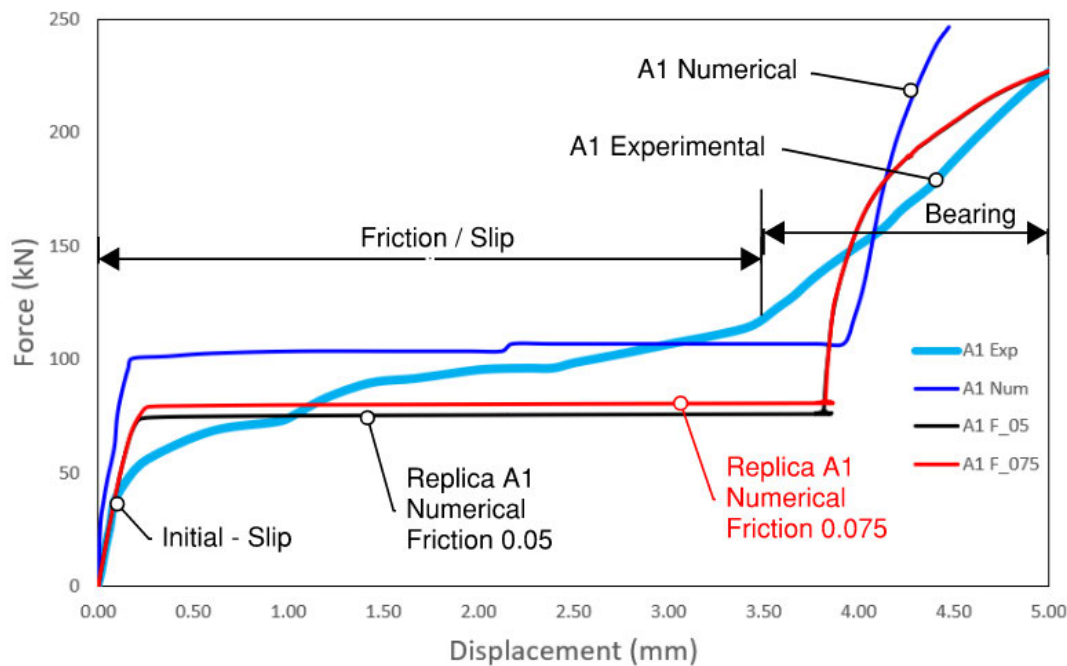
Figure 3.5: Displacement vs Shear force validation by comparison between experimental and numerical results, Modified from Lacey (2019 a)

4.11   Mesh sensitivity studies

Mesh sensitivity studies were conducted on the A1 model using mesh sizes of 6.0, 4.0, 3.0, and 2.0 mm. It was found that the 4.0 mm mesh size produced results similar to the 3.0 mm mesh size and offered faster processing times due to its lower computational cost. The 2.0 mm mesh size provided the most accurate results however, the processing time was 40% slower than that of the 4.0 mm mesh due to the higher computational cost. Therefore, the 4.0 mm mesh size has been selected as the most efficient mesh to length ratio, while still providing accurate results.
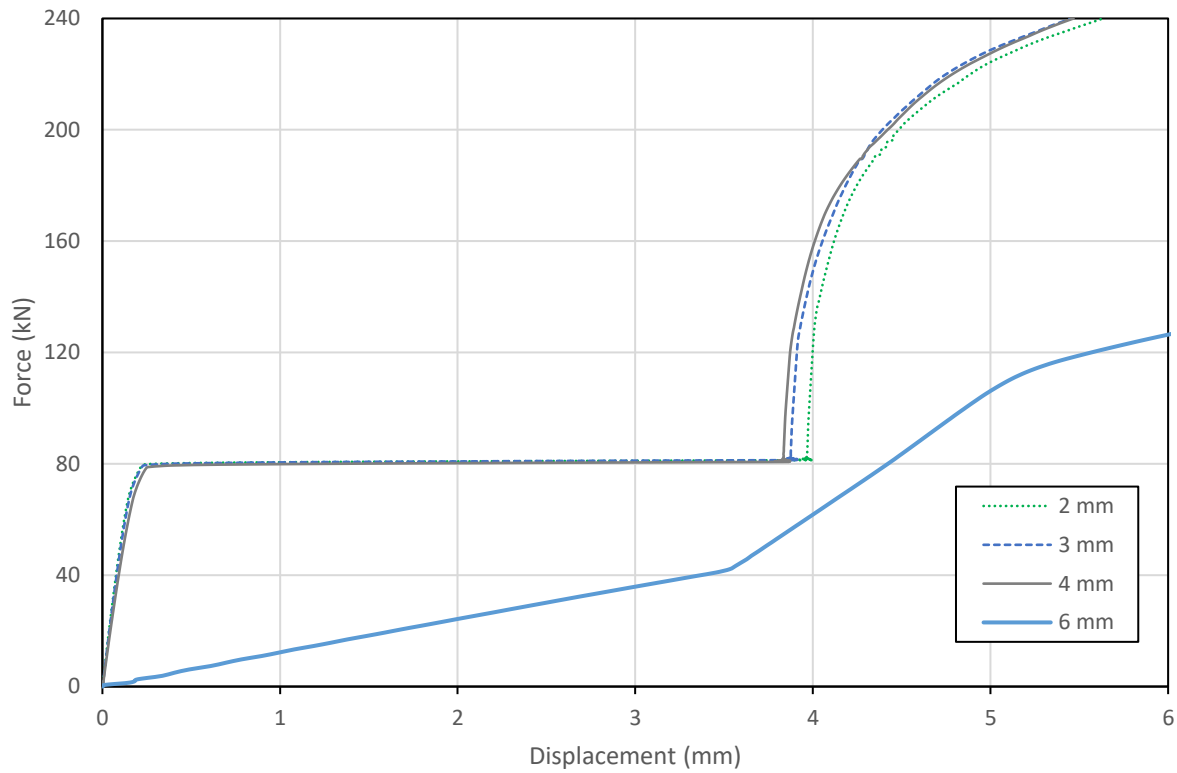
Figure 3.6: Mesh sensitivity analyses for A1 replica model

4.12   Validation of the 2C numerical model

The 2C numerical model provided an additional opportunity to validate the settings and parameters established in the numerical program. The 2C replica model is developed based on the replication of the 2C model published by (Lacey et al. 2020) and includes results of the model's behaviour under shear loading scenarios. The shear loading scenario was used to compare the 2C replica model with the published 2C model to validate the results.

Development of the 2C replica model is covered in Ch.3 Methodology. Similar to the A1 replica model, the 2C replica model showed less resistance to slip, with slip occurring at approximately 27 kN, compared to the reference 2C model that developed slip at approximately 33 kN. This consistent trend of 20% less resistance to slip development is observed across different models established using the same settings and parameters.
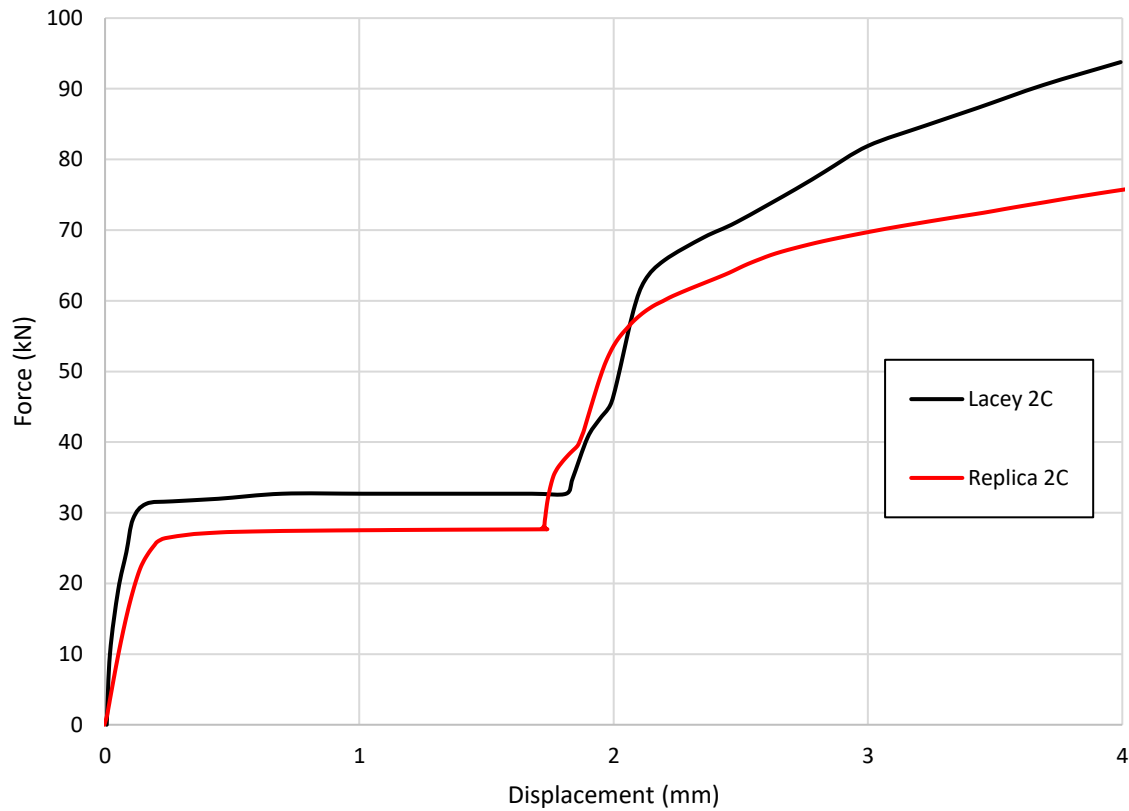
Figure 3.7 Comparison between Lacey's 2C and replica 2C shear force vs displacement.

4.13 Discussion

The results obtained from different models, using the same settings and parameters, have consistently shown similar outcomes. However, there are noticeable differences between the numerical program implemented in the reference papers and the numerical program developed for this research project. The numerical program established in this instance is suitable for the analysis of the numerical models only when compared with models processed in the same program established using the mentioned settings and parameters.

Chapter 5   Development of a Novel Inter-Modular Connection

5.1   Overview

The development of the Novel IMC model is based on the combination of the 2C and P-T IMC models, as published in Lacey et al. (2020 & 2019 b), respectively. The Novel IMC model aims to improve the resistance to slip and gap development between the upper and lower connections. This improvement can be achieved by integrating three geometrical elements found in the 2C and P-T IMCs. These elements include the plates from the 2C IMC model and the shear key and post-tensioned rod from the P-T IMC model.

The Novel IMC model incorporates upper and lower base plates welded to the adjacent columns to interconnect the columns and the IMC. Additionally, there is a central plate with shear keys welded on both sides of the plate. The shear keys on the central plate include 12 mm plates welded at their ends for connection of the post-tensioned rods. These post-tensioned rods tie the IMC into the adjacent columns, providing additional axial resistance.
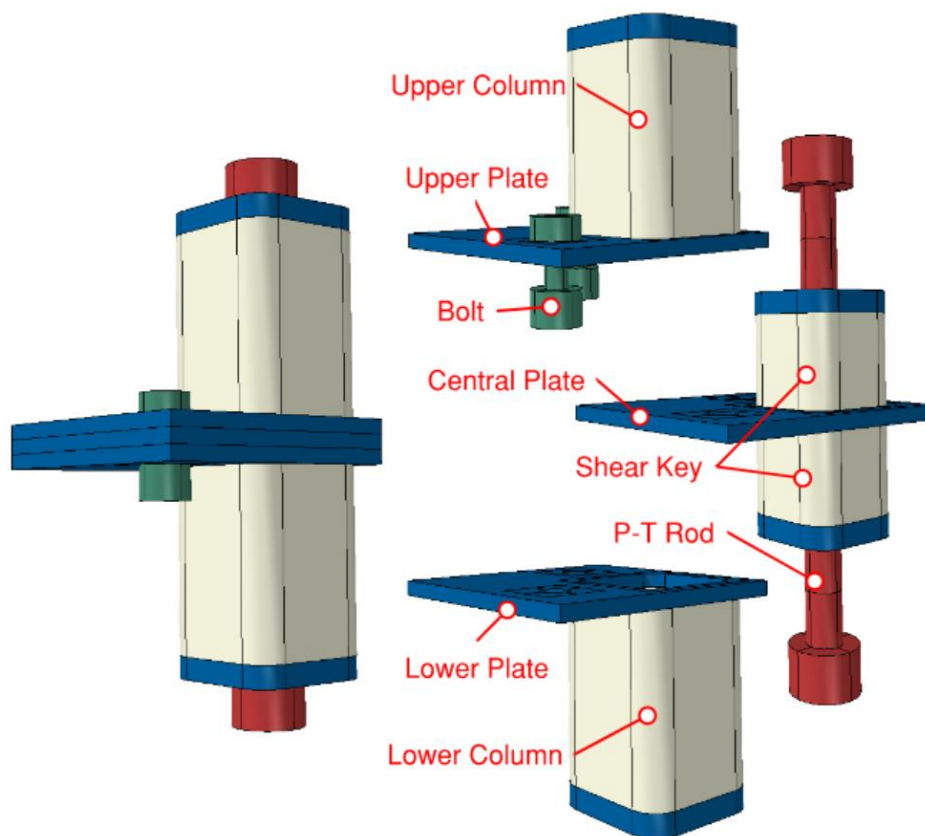
Figure 4.1 Novel IMC model and exploded parts view

5.2 Numerical Model Development.

The Novel IMC model was developed in the FEA program ABAQUS corresponding with all other models developed in this project. This maintains equivalent numerical modelling for comparative analyses of the different model's behaviour under established loading scenarios.

Geometry

The geometry of the Novel IMC model incorporates components replicated from the 2C and P-T models. While most of these components maintain their original geometrical identities from the reference models, some minor adjustments have been made to the geometry to accommodate the development of the Novel IMC model. The Novel model comprises three major components: an upper column welded to a plate, a lower column welded to a plate, and a central plate with shear keys welded to both its upper and lower faces. These shear keys have 12 mm plates welded to their outer ends to facilitate the connection of post-tensioned rods. These post-tensioned rods extend from both sides of the connection and tie into anchors positioned midway along the columns. Finally, the Novel IMC model represent a quarter section of a full model including 2 columns compared to a full section including 8 columns as seen in figures 5.2 & 5.3 below.
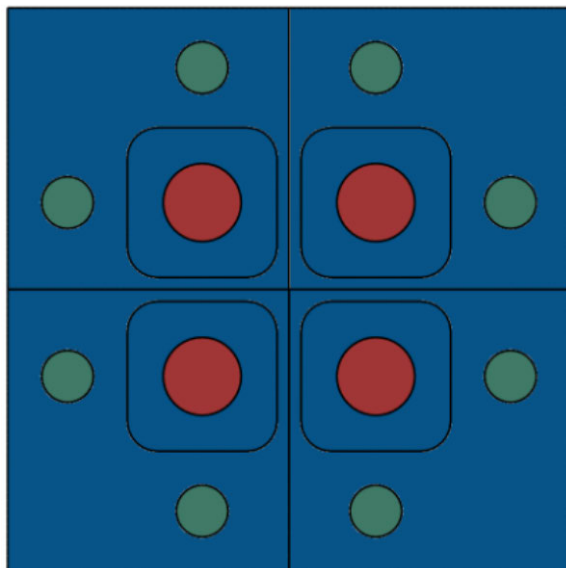
Figure 4.2:Novel IMC Top view, full section
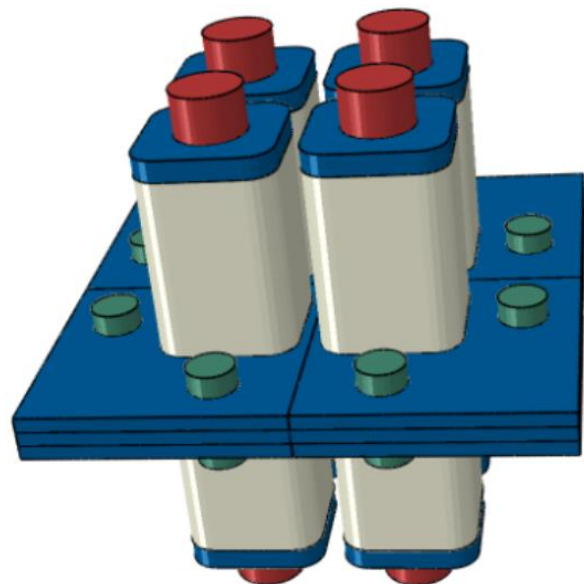
Figure 4.3Novel IMC ISO view, full section

5.2.1 Plate and Column section

The upper and lower plates on the Novel connection maintain an 8 mm thickness, consistent with the 2C model. However, the Novel model's plates measure 141 mm^2, whereas the 2C model's plates measure 135 mm^2. The increase in size, from 135 mm to 141 mm, is intended to accommodate a 6 mm fillet weld around the base of the column, which will join the column with the base plate. Furthermore, the 6 mm extension of the plate serves to create a 12 mm gap between adjacent columns. The provision of a 12 mm gap reduces the likelihood of the columns coming into contact and causing wear on each other. This, in turn, enhances the durability of the columns by minimizing wear on the protective coating and preventing moisture buildup between the columns, which could promote corrosion. The columns for this Novel model match both the 2C and P-T models, with equivalent dimensions of 75 x 75 mm in length and width and a 6 mm thick wall. However, the lengths vary slightly among the 2C, P-T, and Novel models, measuring 50 mm, 69 mm, and 100 mm, respectively, to accommodate the different configurations of these models. Additionally, 12 mm plates are welded to the ends of the columns to facilitate the connection of the P-T rod between the shear key and the outer columns.
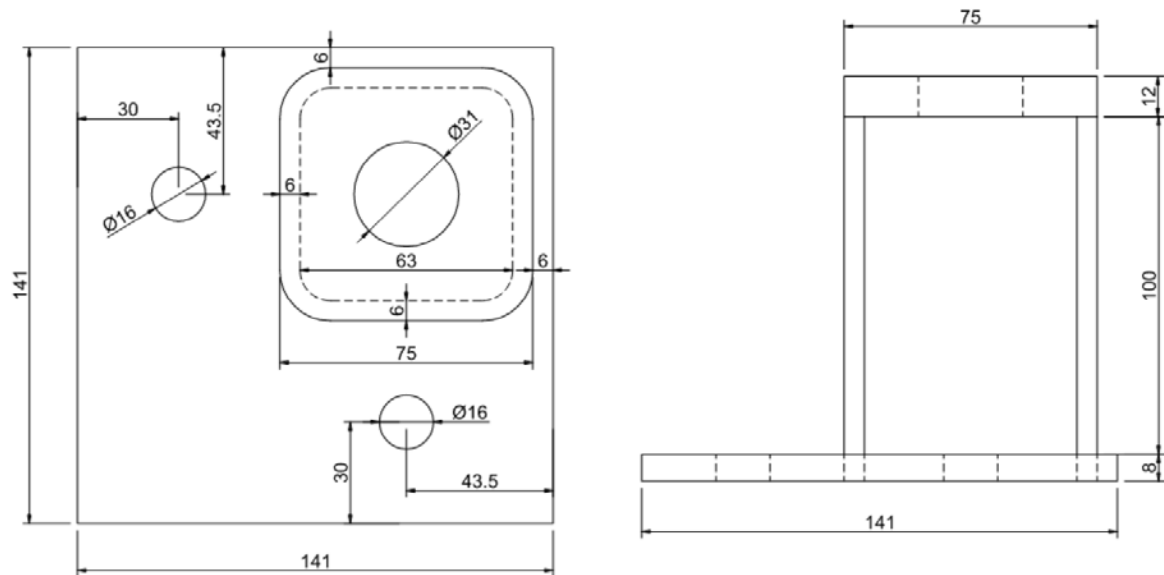
Figure 4.4: Novel IMC - Plan view - Upper section

5.2.2   Shear Key and Central Plate

The central plate maintains an equivalent geometry to that of the upper and lower plates, with a matching plate thickness of 8 mm, consistent with both the 2C and P-T models. The shear key also maintains equivalent dimensions, corresponding to the shear key on the P-T model: 69 x 69 x 6 mm SHS with a length of 50 mm. Additionally, the shear key includes a 12 mm thick cap plate on the outer ends to tie the post-tensioned rods into the connection.
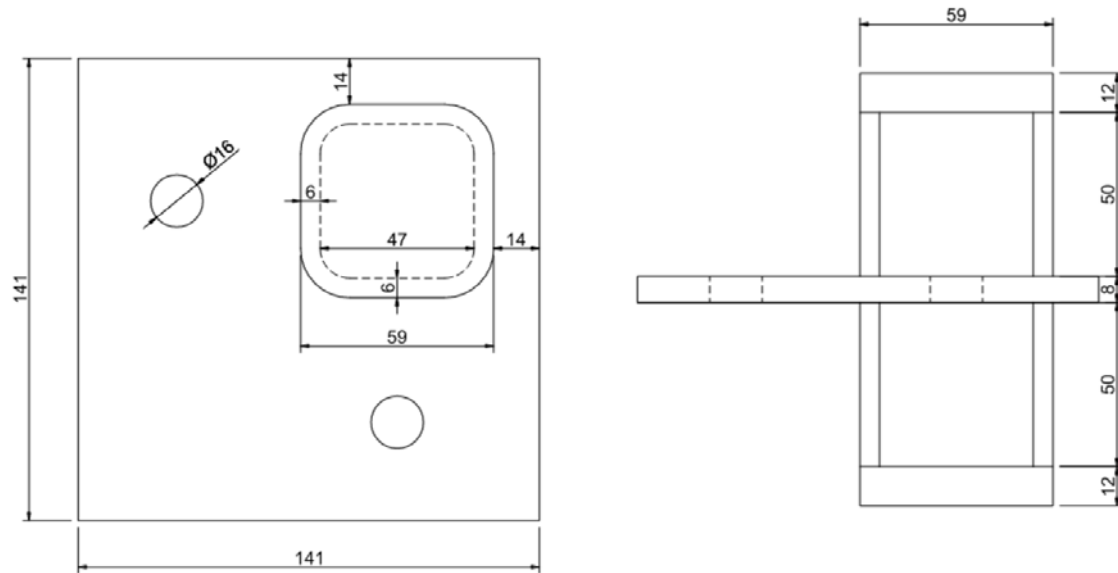
Figure 4.5: Novel IMC - Plan view - Shear key section

5.2.3   Post Tensioned Rod

The post-tensioned rod is responsible for transferring tensile force between the Novel IMC and the adjacent columns. The rod diameter has been matched with a 20 mm diameter to correspond with the post-tensioned rod from the P-T model in Lacey et al. (2019b). To replicate the Novel model's behaviour as a connection system and not an entire modular assembly, the P-T rod only extends to the outer column plates. The post-tensioned rod selected for this IMC model is based on the carbon steel rod listed in Ronstan (2023).
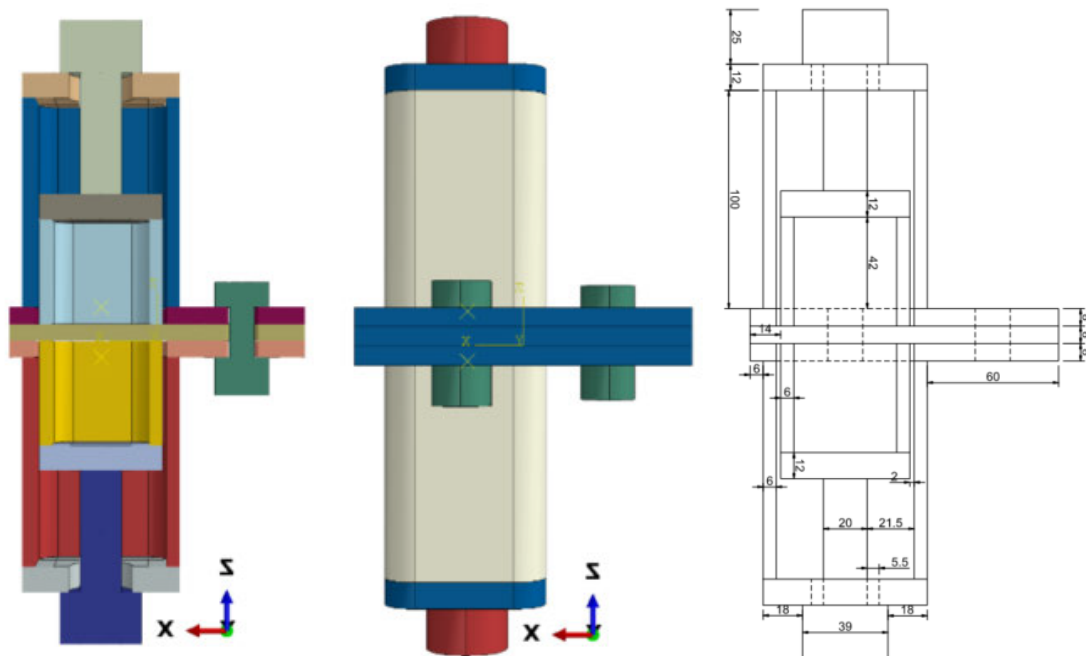
Figure 4.6: Novel IMC model and plan view.

5.3   Material Properties

The material properties for all of the parts correspond to the 2C and P-T models and are listed in Chapter 3.0, (Material Properties), with one exception provided for the post-tensioned rod, as specified in Ronstan (2023). The post-tensioned rod has a modulus of elasticity of 205 GPa and a Poisson's ratio of 0.25. Material property calculations are provided in Appendix B.

Description	Min yield stress (MPa)	Min tensile strength (MPa)	Min elongation (%)
Post tensioned rod (Novel IMC)	520	660	19

Table 4-1: Material Properties of post-tensioned rod, Adapted from: Ronstan. (2023)

5.4   Interaction Properties

The interaction properties for all of the surface pairs correspond with the 2C and P-T models and are listed in Ch. 3.0, Interaction properties and Table 3-2. One additional interaction pair was included for the post-tensioned bolt to column plate pair. These surface pairs are taken as frictionless to simulate the behaviour of the post-tensioned rod acting without any axial resistance.

5.5   Meshing

The meshing is consistent with all other models established in this research project, comprising of first order 8 node linear brick elements at 4 mm average mesh size. Additionally, the bolts and P-T rod are meshed using a wedge style array with a reduced mesh sizing of 3 mm to suit the non-linear geometry of these parts.
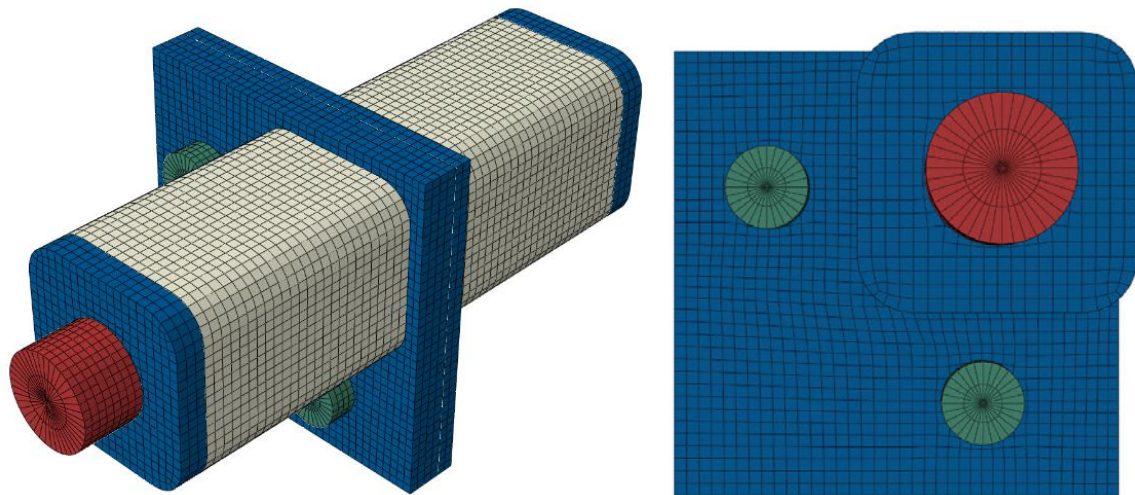
Figure 4.7: Novel IMC Mesh layout

5.6   Parametric Analyses

5.6.1   Verification of IMC Model

To simulate the behaviour of the Novel IMC model, the design was modified to allow the post-tensioned rod to connect to the outer column. This was achieved by adding a 12 mm plate to the end of the outer column, enabling the P-T rod to transfer the tensile force between the shear key and the outer column. However, in a complete modular assembly, the P-T rod extends at least halfway through the column to connect into an anchor. This allows the P-T rod to transfer the tensile forces between the connection and the column. To validate the behaviour of the proposed Novel IMC model compared to the Novel IMC operating within a complete assembly, an additional model was established to replicate the behaviour of a complete modular assembly. The verification IMC model extends the outer columns and the P-T rod to a length of 1500 mm and connects the P-T rod to the column's end plate, to replicate a full-scale modular column section.

Both models were simulated under the same shear loading scenario with equivalent restraint and loading geometry. The results were graphed in the same table for comparison and evaluation. A visual inspection of the combined graphs verifies that the Novel IMC model behaves almost identical to the Verification model. Therefore, the results provided by the numerical Novel IMC model will offer credible information and data for assessing the behaviour of the connections under a range of loading scenarios.

Figure 4.8: Novel IMC extended column model.
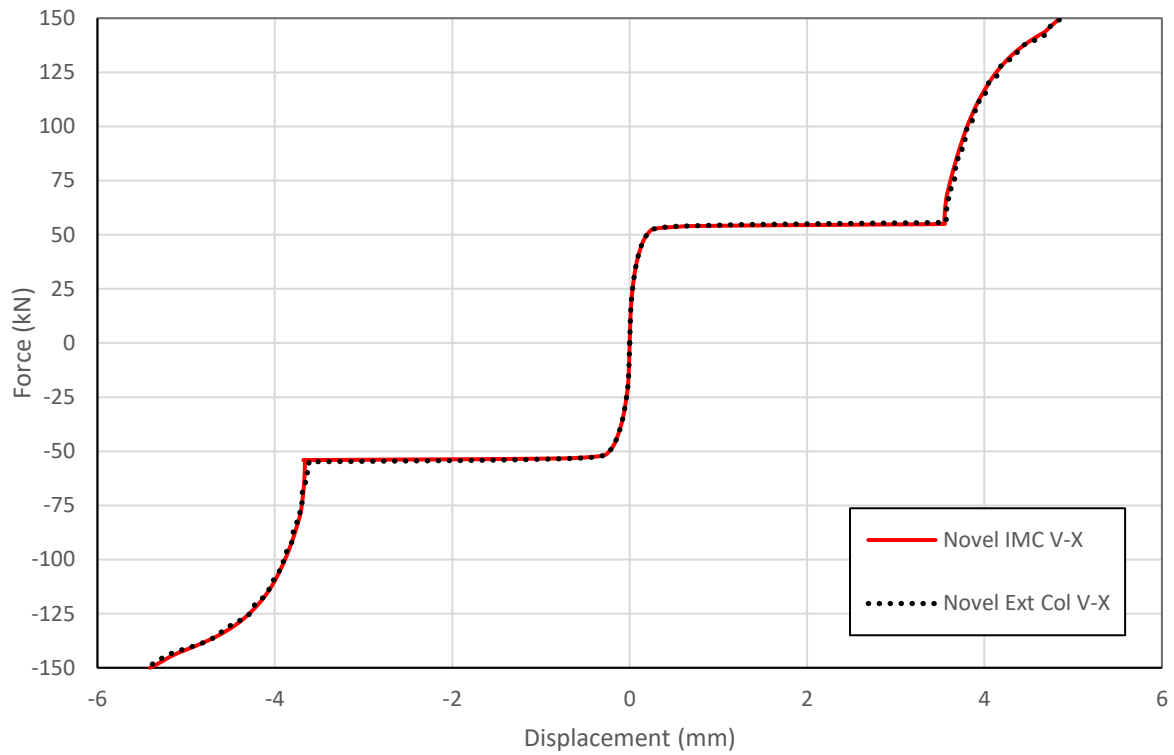
Figure 4.9 Verification of the Novel IMC model vs extended column model.

5.6.2   Post Tensioned Pre-load

A parametric analysis was conducted across a range of tension values applied to the P-T rod to assess its impact on the connection system. The preloading magnitude was adjusted in 18.75 kN intervals, ranging from 0.0 to 93.25 kN. The results for different P-T tension values confirm an increased resistance to slip development under applied shear force.
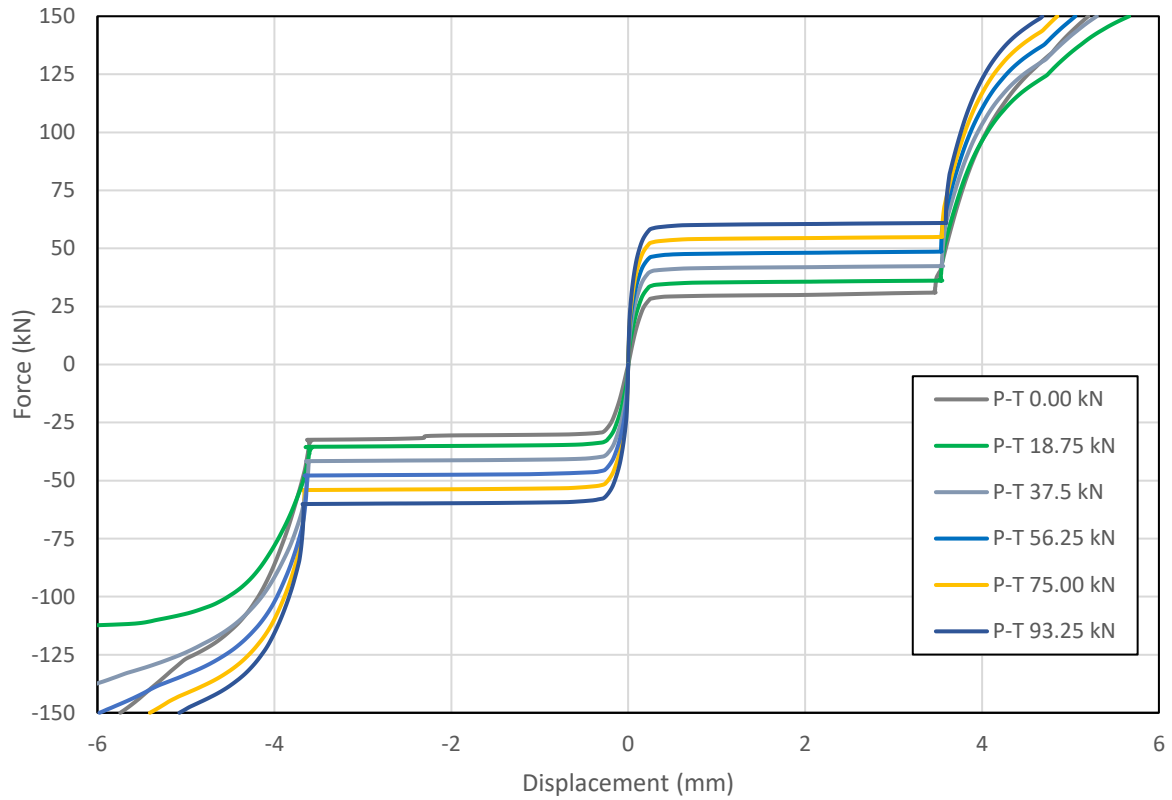
Figure 4.10: Parametric analyses for varying post-tensioned magnitudes.

5.7   Discussion

The Novel IMC model has been established to integrate aspects of both the 2C and P-T models. However, in order to incorporate the post-tensioned rod in the numerical model, the geometry must be modified to accommodate it. Therefore, two separate analyses were conducted on the numerical Novel IMC model to confirm its behaviour. The extended column model verified that the Novel IMC model behaves consistently with a full-scale model. While a parametric analysis confirmed that the post-tensioned rod significantly influences the response of the Novel IMC to applied loading. Therefore, the Novel IMC model offers a credible simulation for analysing this model in comparison to the other 2C and P-T models across various loading scenarios.

Chapter 6 Analyses and Results

6.1 Overview

This chapter covers the loading scenarios applied to three models: the P-T, 2C, and Novel IMC models. A range of equivalent loading scenarios is applied to each of the models to reveal and compare their behaviour. The magnitude of the loads is applied relative to the displacement and yield strengths in each model to facilitate a comparison among the different models.

6.2 Analyses Scenarios

For the analyses and comparison of the individual IMC models, the restraints and loading conditions were established to correspond between the different models. The geometrical allocation of the restraints and loading conditions is detailed in Chapter 3, Table 3-4.

6.2.1 Restraint

A fixed restraint was applied through a reference point connected to the top of the lower columns. The establishment of this restraint is equivalent in all three models and is detailed in Figures 3.13, 3.14 & 3.15.

6.2.2 Shear (V) Loading

Shear loading was applied to the web of the upper column through a reference point connected centrally to the column webs as detailed in Figures 3.16, 3.17 & 3.18. The displacement and applied force at the reference point were recorded and extracted to establish the displacement vs. force graphs. For the Replica 2C and Replica P-T models, a 100 kN shear force was applied, while the Novel IMC model was subjected to a 150 kN shear force. These values correspond to the yield strengths of the IMC models.

6.2.3 Axial (N) Loading

An axial load was applied to the top of the upper column through a centrally connected reference point as detailed in Figures 3.19, 3.20 & 3.21. The displacement and applied force at the reference point were recorded and extracted to establish the displacement vs. force graphs. The axial load was applied in the positive upward direction and incrementally increased to 50 kN for the replica 2C model, 76.5 kN for the replica P-T model and 150 kN for the Novel IMC model. These values correspond to the yield strengths of the IMC models.

6.2.4 Moment (M) Loading

A bending moment was applied to the top of the upper column through a centrally connected reference point as detailed in Figures 3.22, 3.23 & 3.24. Displacements were recorded at points three and four to establish the rotation of the upper column about the z-axis.

The rotation in Radians can be expresses by

$$\theta_z = \tan^{-1}\left(\frac{y_3 - y_4}{b_{col} + x_4 - x_3}\right) \qquad \text{Lacey et al. (2020)}$$

Such that y_3 and y_4 are the vertical displacements of points 3 and 4 respectively, x_3 and x_4 are the horizontal displacements of points 3 and 4 respectively, and b_{col} is the width of the column Lacey et al. (2020).

Loading magnitudes of 2.0, 4.0 and 9.0 kNm were applied in the positive directions and -6.0, -4.0 and – 11.0 kNm in the negative directions to the 2C, P-T and Novel IMC models respectively. These values correspond to the yield strengths of the IMC models.

6.2.5   Shear + Axial (V + N) Loading

A combined shear and axial loading were applied to the replica 2C and Novel IMC models. Shear loading was applied first to the column web, after which an axial load was applied to the top of the upper column. The replica 2C model had a shear loading of 15 kN applied in the positive x-direction after which an axial loading of 50 kN was applied in the upward axial direction with the shear loading propagated into the axial loading stage. The Shear loading is then applied in the negative x-direction with an axial load of 50 kN applied in the upward axial direction and the shear loading propagated into the axial loading step.

Similarly, the above combined loading case was applied to the Novel IMC model, however an increased axial load of 100 kN was applied to create obtain similar displacement for comparison and review.

6.2.6   Moment + Axial (V + N) Loading

A combined bending moment and axial loading were applied to both the replica 2C and Novel IMC models. Initially, a bending moment was applied to the top of the upper column, followed by the application of an axial force to the same location. In the case of the replica 2C model, a positive bending moment of 0.79 kNm was applied in the positive direction, followed by a compressive axial force of -80 kN. This process was then repeated with a tensile axial force of 30 kN. Subsequently, a negative bending moment of -2.3 kNm was applied, followed by the previously mentioned axial load values.

Similarly for the Novel IMC model, a positive bending moment of 0.79 kNm was applied in the positive direction, followed by a compressive axial force of -80 kN. This process was then repeated with a tensile axial force of 150 kN. Subsequently, a negative bending moment of -2.3 kNm was applied, followed by the previously mentioned axial load values.

Table 5-1: Loading cases for 2C, P-T & Novel IMC models.

Loading Case	Model		
Shear (V)	2C	P-T	Novel
	V (kN)	V (kN)	V (kN)
Positive	100.0	80.0	150.0
Negative	- 75.0	- 80.0	- 150.0
Axial (N)	2C	P-T	Novel
	V (kN)	V (kN)	V (kN)
Positive	50.0	76.5	150.0
Negative	NA	NA	NA
Moment (M)	2C	P-T	Novel
	M (kNm)	M (kNm)	M (kNm)
Positive	2.0	4.0	9.0
Negative	- 6.0	- 4.0	- 11.0

Loading Case	2C		P-T	Novel	
Shear - Axial (V+N)	2C		P-T	Novel	
	V (kN)	N (kN)		V (kN)	N (kN)
Positive	+15.0	+50.0		+15.0	+100.0
Negative	-15.0	-50.0	NA	-15.0	-100.0
Moment - Axial (M+N)	2C		P-T	Novel	
	M (kNm)	N		M (kNm)	N (kN)
Positive	0.79	30.0 / -80.0	NA	0.79	150.0 / -80.0
Negative	-2.3	80.0 / -80.0		-2.3	150.0 / -80.0

6.3   Shear (V) Loading

6.3.1   2C Replica

Under the applied horizontal bearing load, the 2C replica model showed minor displacement in the horizontal direction, up to 0.15 mm, due to material yielding. This occurred until the slip resistance was exceeded at around 25 kN, causing the two plates to begin slipping. The plates continued to slip displacing by 2 mm until the tolerance of the bolt holes was exceeded, and the bearing forces were transmitted between the bolt and the plates. The bolt and pins support the bearing load up until they yield at approximately 50 kN, after which plastic deformation occurs, resulting in significant displacement of the plates.

6.3.2   P-T Replica

The P-T replica model showed similar resistance to the horizontal bearing load up to approximately 25 kN, after which the slip resistance is exceeded, and the plate slips between the columns, displacing by 4 mm until the gap between the columns and shear key is exceeded. The bearing force is transmitted into the shear key and ultimately taken up by the P-T bolt, which yields at around 65 kN, resulting in a loss of yield strength and allowing for significant displacement to occur between the upper and lower columns.

6.3.3   Novel IMC

The Novel IMC model demonstrates improved resistance to horizontal bearing loads. Slip occurs at approximately 53 kN, followed by a 3.55 mm displacement. This displacement continues until tolerances between the bolts, plates, shear key, and column are exceeded. The bearing force is transmitted through the bolts and plates, as well as the shear keys, P-T rods, and columns.

Under positive shear loading, the forces are transmitted through the plates and into the bolts as a tensile axial force. The behaviour of the model is determined by the capacity of the plates and bolts. In contrast, under negative shear loading, the forces are distributed throughout the

plates and bolts, as well as through the P-T rod, as a tensile axial force. The ultimate capacity of the P-T rod determines the behaviour of the model.
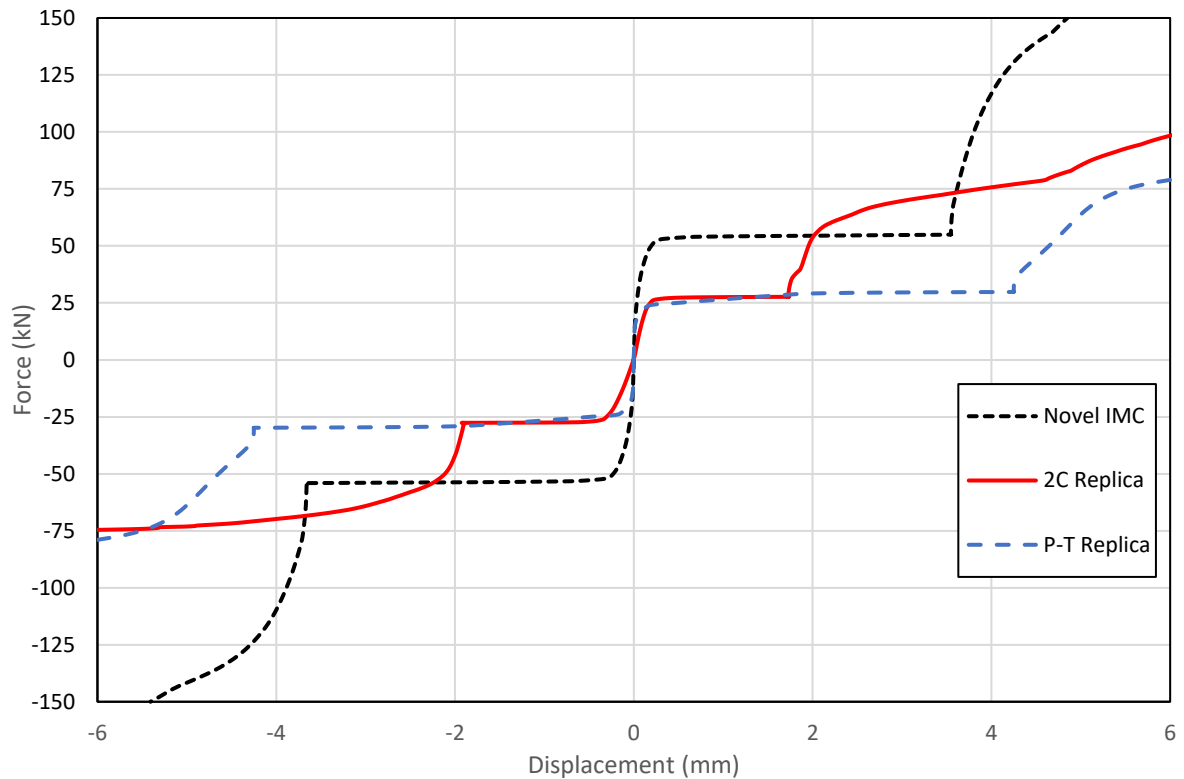

Figure 5.1: Displacement vs shear force with 2C Replica, P-T Replica and Novel IMC plots.

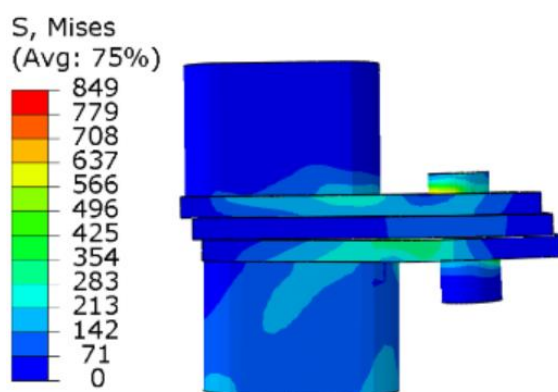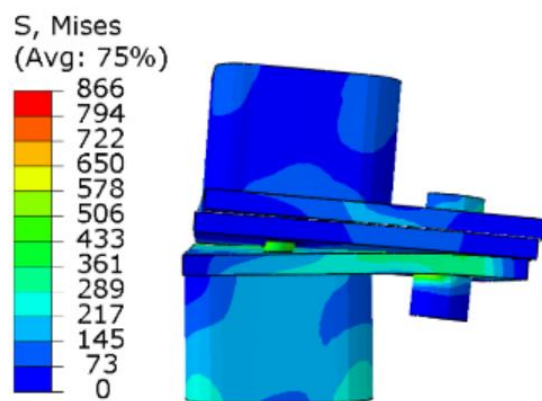*Figure 5.2: 2C Positive V-X 100 kN*
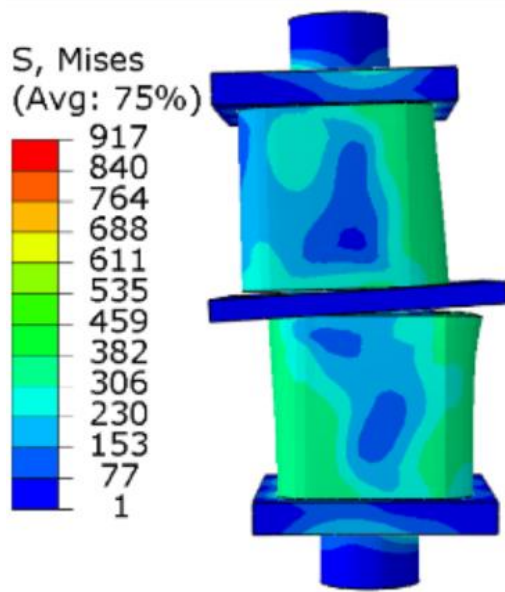
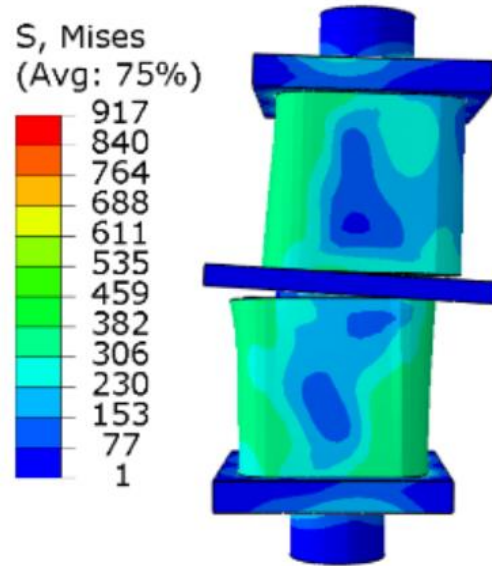*Figure 5.3: 2C Negative V-X 75 kN*

Figure 5.4: P-T Positive V-X 100 kN
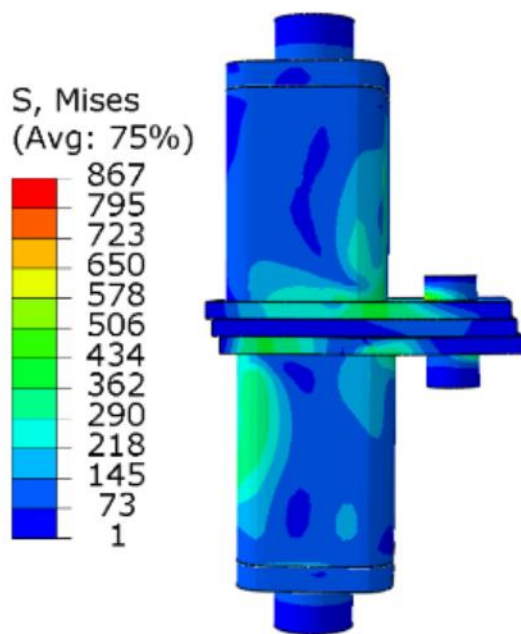

Figure 5.5: P-T Negative V-X 100 kN
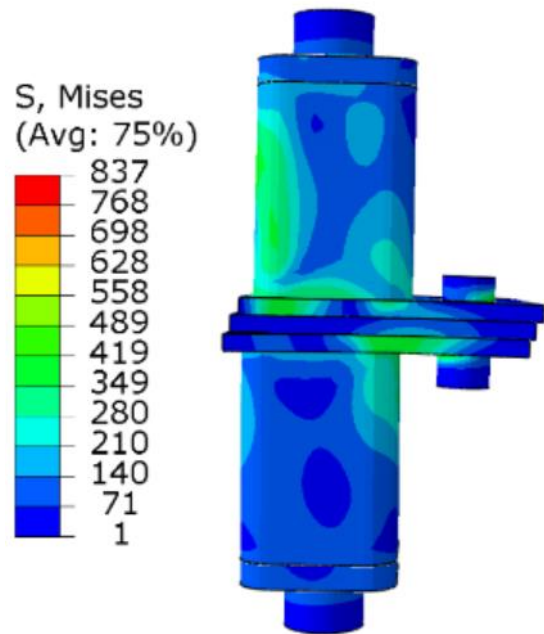

Figure 5.6: Novel IMC Positive V-X 150 kN

Figure 5.7 Novel IMC Negative V-X 150 kN

6.4 Axial N-Z loading

6.4.1 2C Replica

The 2C replica model provides resistance to tensile axial loading by connecting the plates with a pair of bolts. The plates begin to deform when axial load is applied, which determines the behaviour of this model under such loading conditions. The results indicate that the 2C model has lower resistance to axial loading, with axial displacement occurring as soon as the tensile load is applied.

6.4.2 P-T Replica

The P-T replica model exhibits straightforward behaviour in resisting axial loading, with the P-T rod solely responsible for bearing this load. It is evident that the P-T model offers higher resistance to tensile axial loading, with no displacement occurring until approximately 75 kN. However, after the onset of displacement, once the yield strength degrades, the P-T rod fails catastrophically without offering any plastic resistance. This behaviour is dangerous for any structural system to exhibit since it does not provide any warning to the users.

6.4.3 Novel IMC

The Novel IMC model demonstrated enhanced resistance to tensile axial loading, with no displacement occurring until it reached approximately 75 kN. At this point the model exhibited plastic deformation due to the bending of the plates. This behaviour effectively provides resistance to displacement up to 75 kN, at which point the plates offer redundant resistance to catastrophic failure. Therefore, this Novel IMC model has provided improved resistance to tensile axial loads while integrating redundancies into the connection.
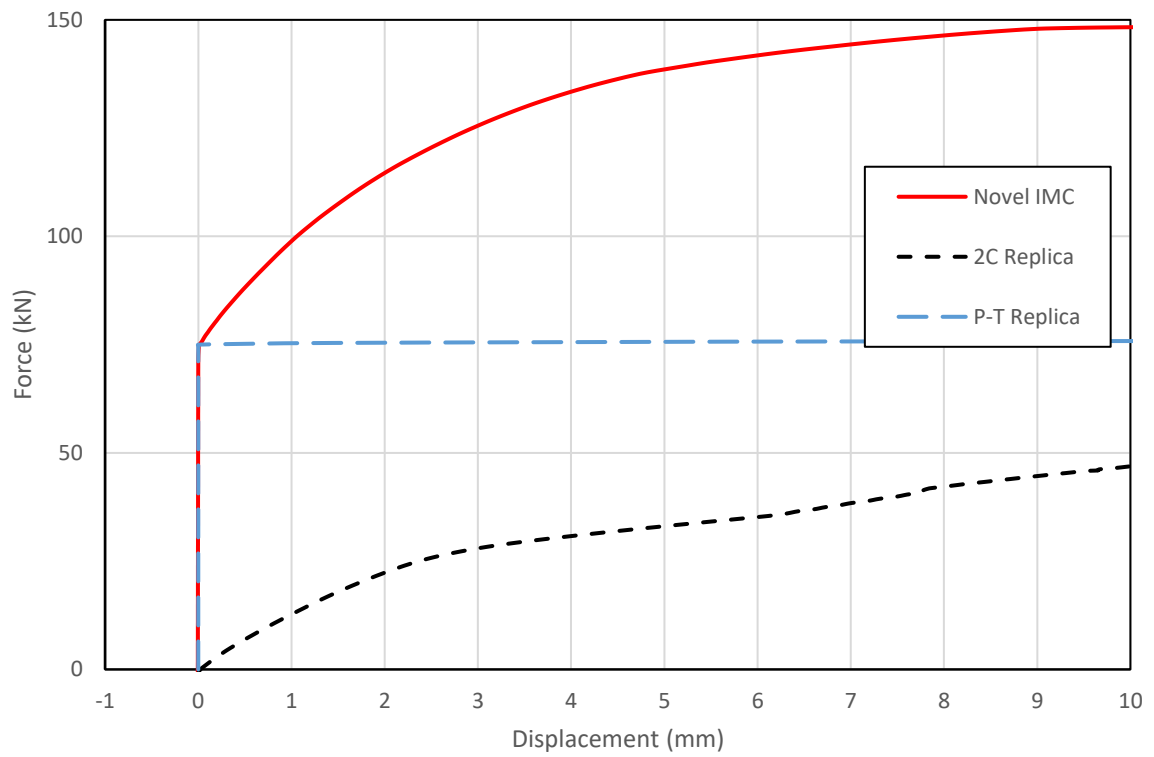
Figure 5.8: Displacement vs axial force with 2C Replica, P-T Replica and Novel IMC plots.
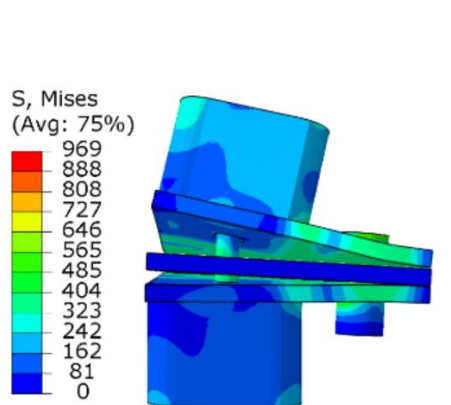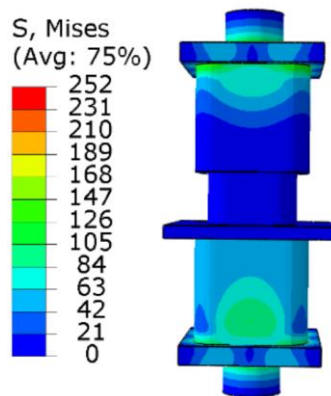

Figure 5.9: 2C Positive N-Z 70 kN
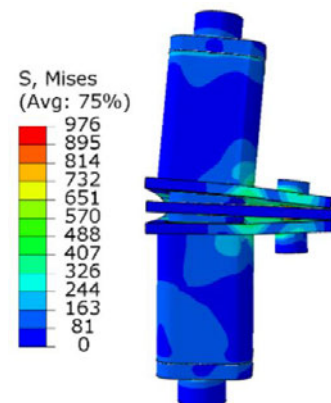

Figure 5.10: P-T Positive N-Z 76.5 kN

Figure 5.11 Novel IMC Pos N-Z 150 kN

6.5   Moment Bending

6.5.1   2C Replica

The reaction of the 2C model to moment rotation differed between positive and negative bending directions. This discrepancy arises because, in the case of positive bending, the only resistance against the bending force comes from the plate's capacity to resist twisting along the yield line, without any secondary support to resist the bending. In comparison, negative bending creates a combined bending and tensile action on the plate. In this scenario, the plate bends upwards between the bolt and the column, while the other side of the plate presses down on the central plate. These different structural behaviours result in the upper column rotating approximately 0.12 radians under a positive bending moment of 2 kNm, whereas it rotates approximately 0.12 radians under a negative bending moment of 6 kNm.

6.5.2   P-T Replica

The application of a bending moment to the P-T model exhibits straightforward behaviour similar to that of a tensile axial load. The bending moment creates a tensile axial force on the P-T rod, and as a result, the structural capacity of the P-T model depends on the ultimate bearing capacity of the P-T bolt. Similar to the axial behaviour, this model does not provide any plastic resistance and fails catastrophically after the yield strength degrades. This behaviour is equivalent for positive and negative bending moment loads due to the symmetrical geometry of the P-T model.

6.5.3   Novel IMC

The Bending moment loading scenario reveals improved behaviour in the Novel IMC model. Initially bending in both directions shows similar resistance to the applied force as the P-T model. However, as displacement develops, the yield strength of the P-T rod degrades, and the plates absorb the increasing force. The combined capacity of the P-T rod and plates increase the resistance to displacement up until 2 kNm. After which this point, the model exhibits plastic deformation, that serves as a warning to the loss of structural capacity in the IMC.
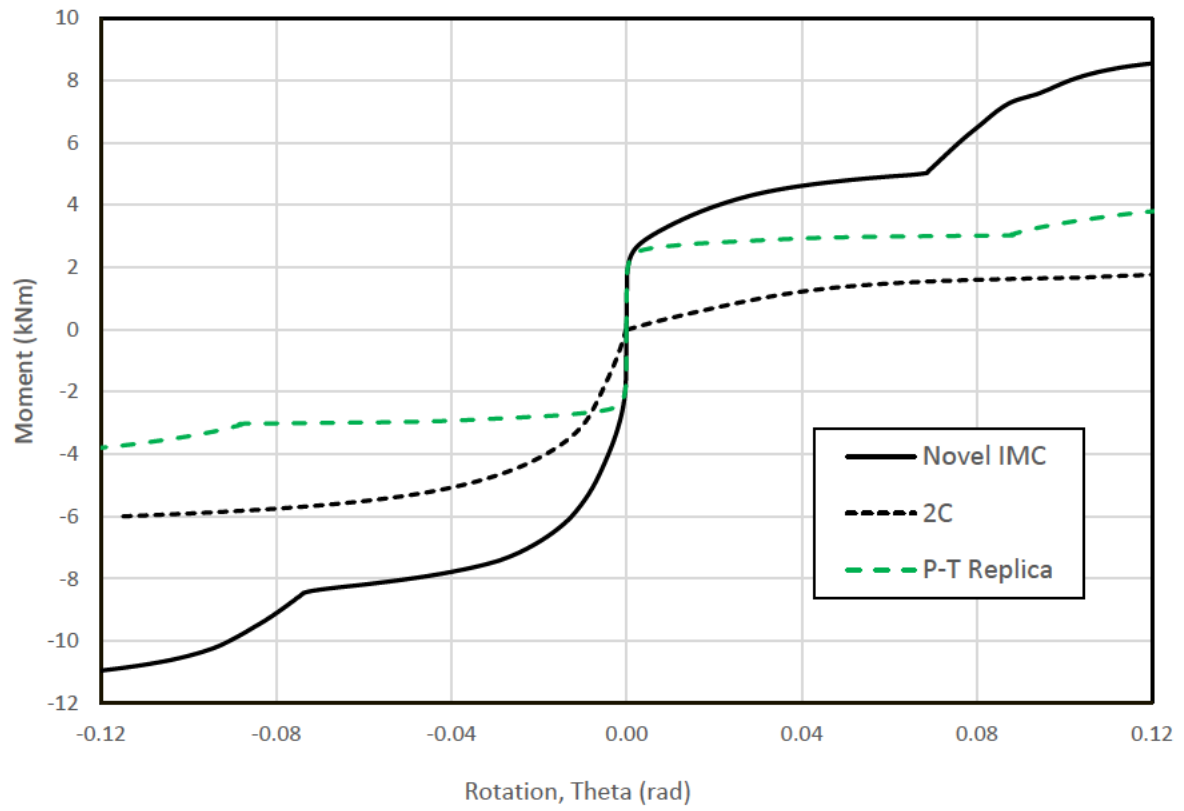
Figure 5.12: Moment vs Rotation including 2C Replica, P-T Replica and Novel IMC plots.
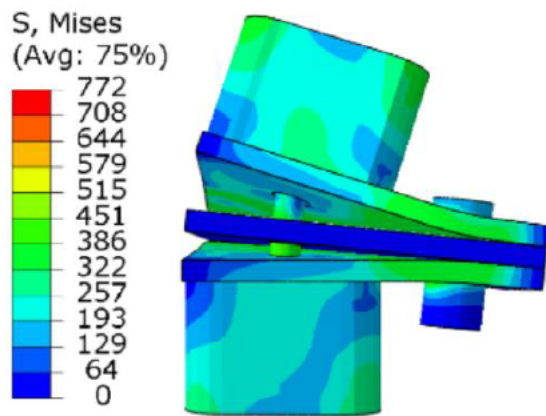

Figure 5.13: 2C Replica Positive moment 2kNm
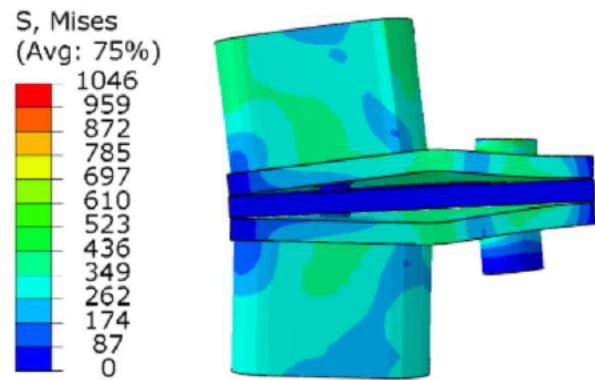
Figure 5.14: 2C Replica Negative moment 6kNm
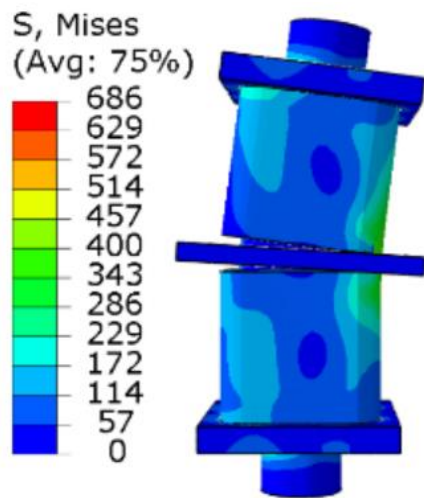
Figure 5.15: P-T Replica Positive Moment 4 kNm
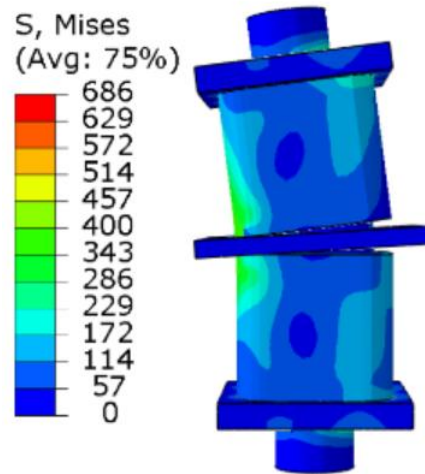
Figure 5.16: P-T Replica Negative Moment -4 kNm
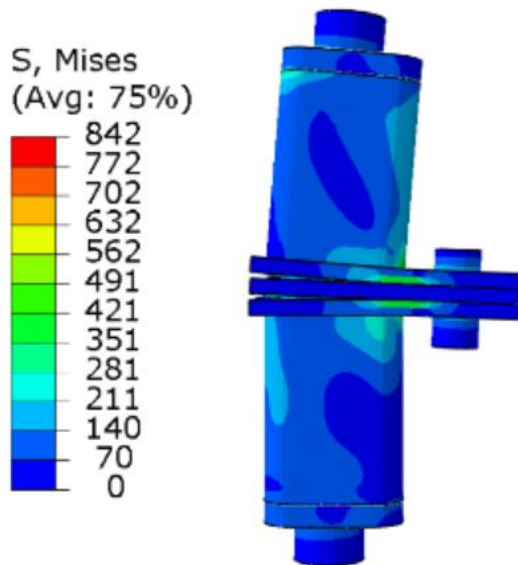
Figure 5.17: Novel IMC positive moment 8 kNm
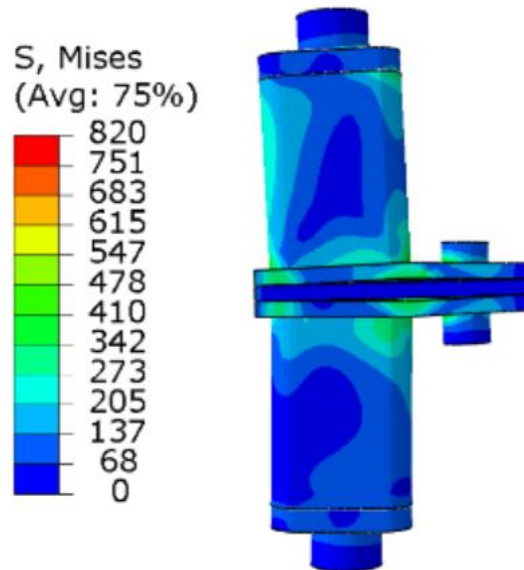
Figure 5.18 : Novel IMC negative moment -10 kNm

6.6 Shear + Axial (V+N)

6.6.1 2C Replica

Applying a shear force in the positive x-direction creates a negative bending moment between the applied load at the upper reference point and the restraint at the lower reference point. This results in the development of a compressive axial force, which slightly increases the axial capacity of the upper column. As a result, the upper column can resist displacement in the z-direction until the axial force exceeds approximately 2.5 kN.

Conversely, applying a shear force in the negative x-direction creates a positive bending moment between the applied load at the upper reference point and the restraint at the lower reference point. This results in the development of a tensile axial force, which slightly reduces the axial capacity of the upper column. As a result, the upper column develops an upward displacement of around 0.25 mm before the axial load is added, leading to a slight reduction in axial capacity.
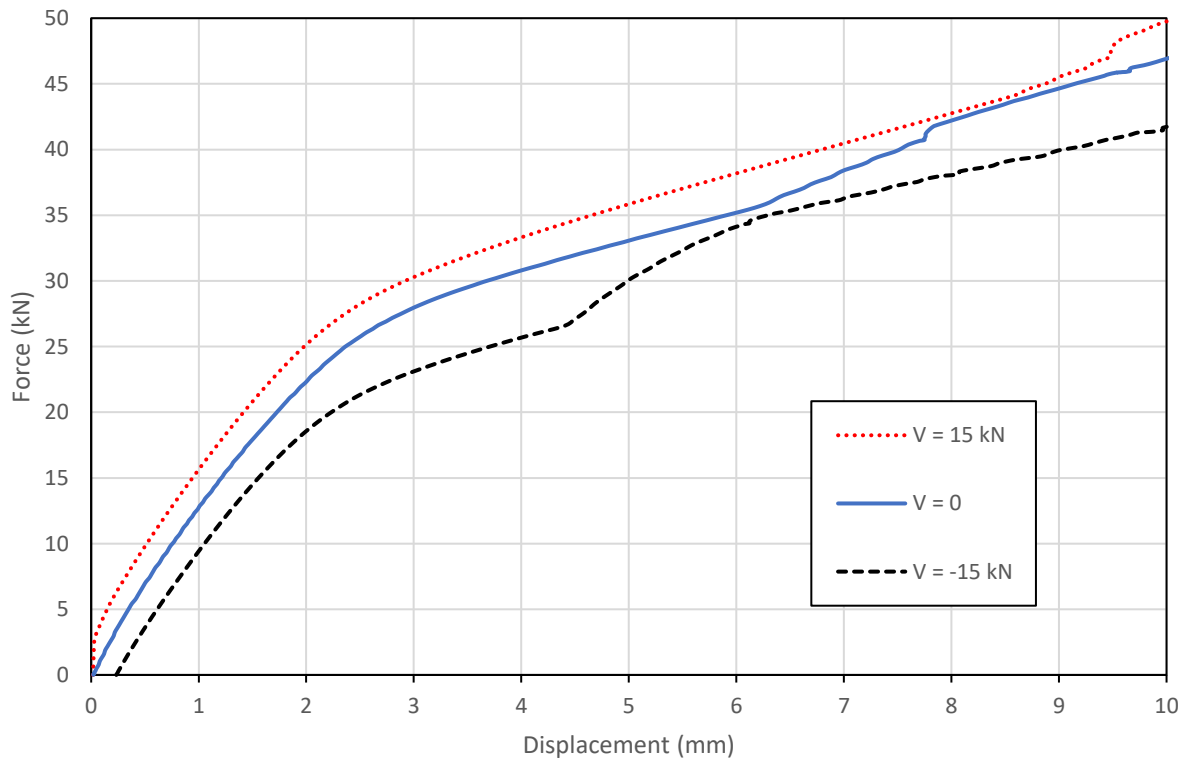
Figure 5.19: Displacement vs axial and shear force combined loading for 2C Replica model.

6.6.2 Novel IMC

The combined loading case against the Novel IMC model closely resembles the behaviour to the 2C model under the same loading scenario. By which the application of the positive shear loading slightly increases the axial capacity while the negative shear loading slightly decreases the axial capacity.
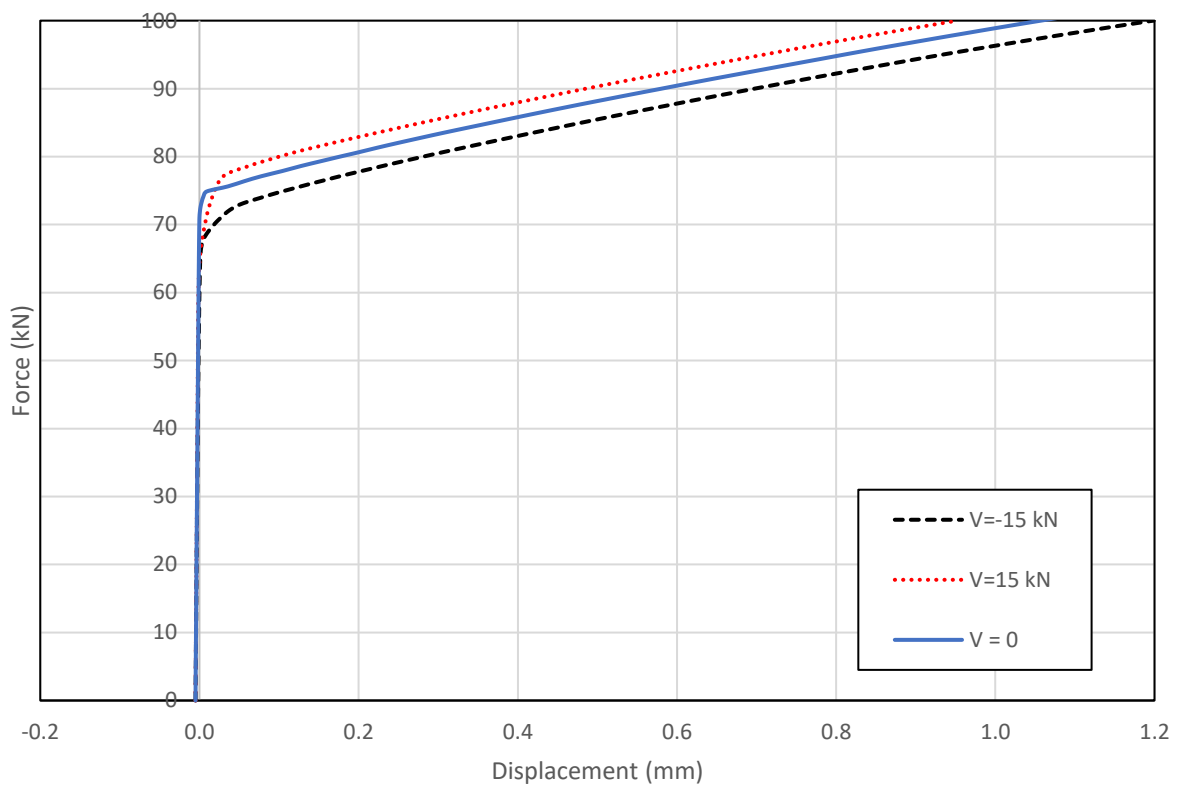
Figure 5.20: Displacement vs axial and shear force combined loading for Novel IMC model.

6.7 Moment + Axial (M + N)

6.7.1 2C Replica

The application of either the positive or negative moment caused the upper plate to deform and introduced upward displacement earlier. Additionally, the positive moment reduced the axial capacity by approximately 12 kN to achieve a similar displacement without the bending moment. On the other hand, applying the negative moment increased the axial capacity by approximately 25 kN to achieve a similar displacement without the bending moment.
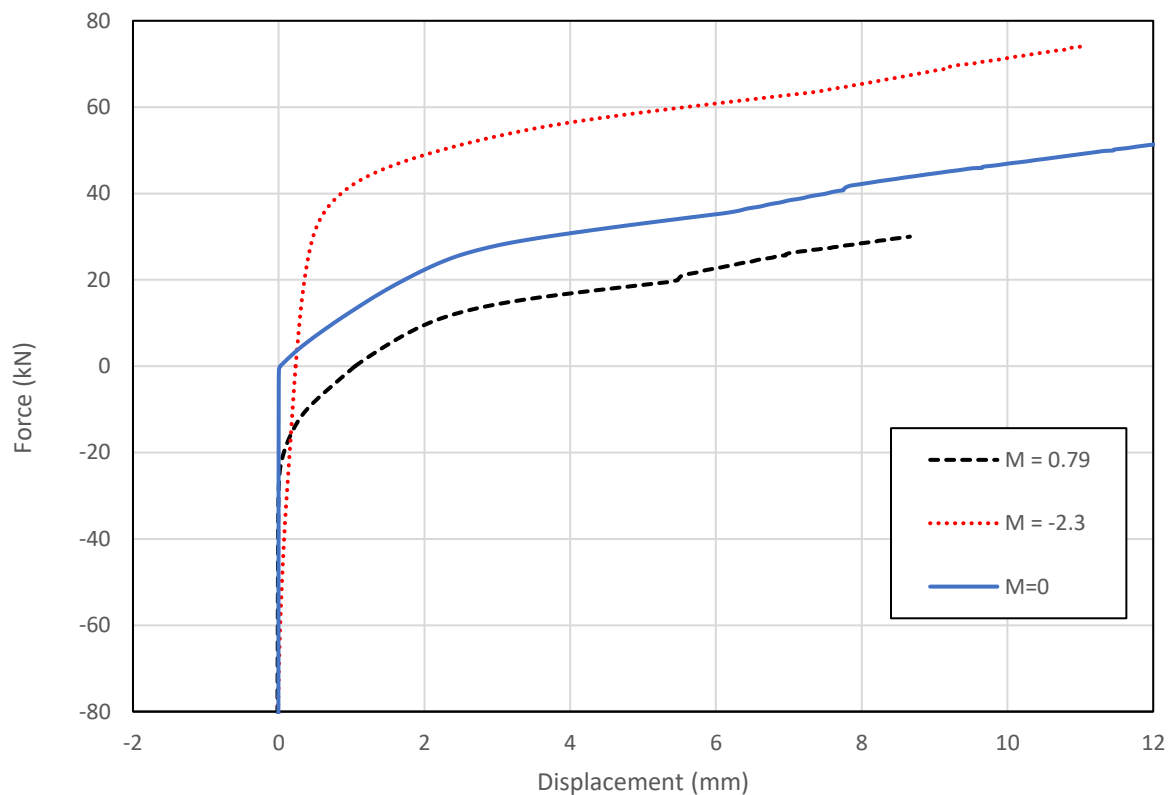
Figure 5.21: Displacement vs axial force and combined bending moment for 2C Replica model.

6.7.2 Novel IMC

Similar to the 2C model, the initial application of a bending moment causes an initial distortion of the upper plate and introduces upward displacement earlier. The positive bending moment reduced the axial capacity by approximately 20 kN compared to without the bending moment. And the negative bending moment increased the axial capacity by around 18 kN.
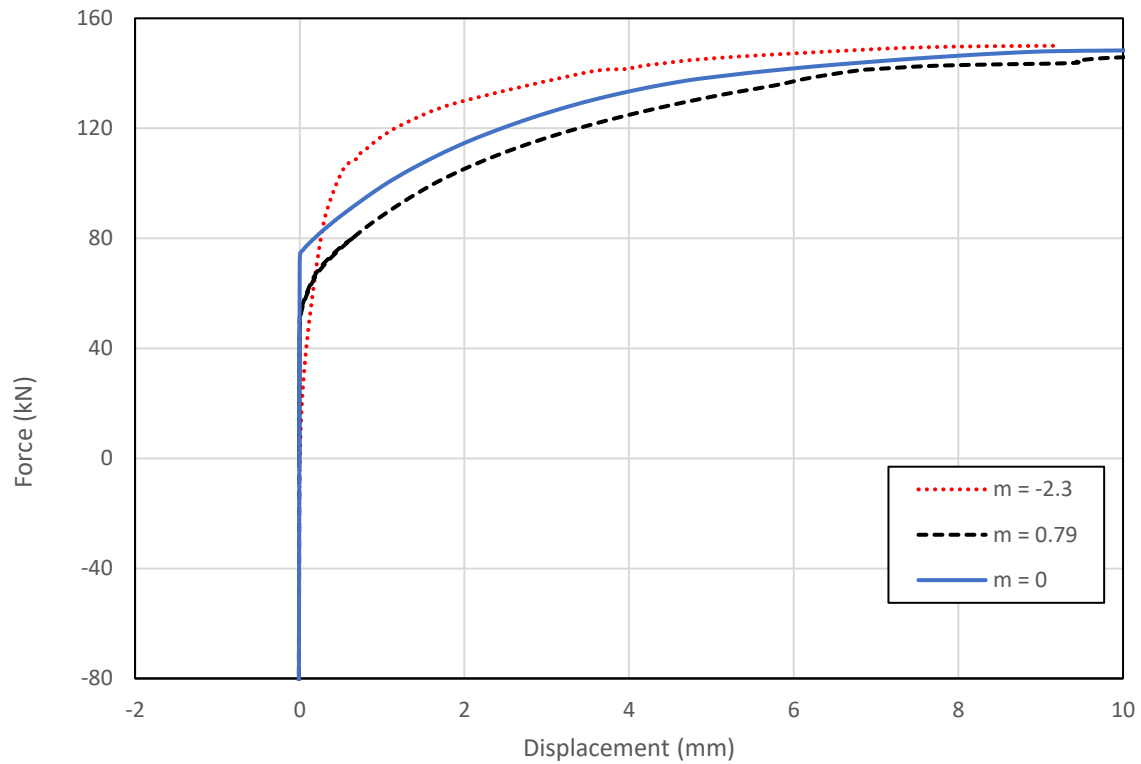
Figure 5.22: Displacement vs axial force and combined bending moment for Novel IMC model.

Summary

The P-T, 2C, and Novel IMC models were subjected to various loading scenarios to assess their behaviour under different conditions. Under pure shear force loading, both the 2C and P-T IMC models developed slip at approximately 25 kN, while the Novel IMC model showed a 100% increase in resistance to slip development, reaching over 50 kN. However, the 2C model only continues to slip up to 2 mm before the gap between the bolt and plates is exceeded. In contrast both the P-T and Novel IMC models continue to slip up until the gap between the shear key and columns is exceeded at approximately 4 mm. Under axial loading both the P-T and Novel IMC models showed greater resistance to the tensile force compared to the 2C model. The 2C model was found to have little resistance to tensile axial loading and immediately develops displacement at the onset of a tensile force. In comparison, both the P-T and Novel IMC models resisted axial displacement up to approximately 75 kN. However, the P-T model failed entirely at that point, while the Novel IMC model continued to provide yield strength through the connecting plates. Under bending moment loading the 2C model showed three times greater resistance to the negative direction compared to the positive direction, due to the geometrical configuration of the plates. In comparison the P-T model provides a symmetrical resistance to displacement in both bending direction with displacement occurring at approximately 2.5 kNm followed by excessive displacement. The behaviour of the Novel IMC model was consistent with the superimposition of both the 2C and P-T models, owing to the combined geometrical identities. This exhibited a non-symmetrical response to bending moments, with resistance of up to 5 kNm in the positive bending direction and -8 kNm in the negative bending direction. The combined loading cases exhibited a consistent trend in both the 2C and Novel IMC models, demonstrating an approximate 100% increase in overall resistance to displacement against the applied load. Consequently, the results unequivocally indicate that the Novel IMC model offers enhanced performance in all loading scenarios, while providing additional redundancy to resist catastrophic failure.

Chapter 7   Conclusions

This chapter will conclude the study by summarising the key research findings in relation to the research aims and objectives, as well as assessing the value and contribution of the research to the industry. It will also review the limitations of the research and propose opportunities for further research in future investigations.

7.2   Achievement of Aims and Objectives

This study aimed to develop an improved Novel IMC model based on the combination of two existing IMC models. The Novel IMC model was developed along with two existing IMC models published by (Lacey et al. 2019b and 2020) and an additional (A1) model for numerical program validation. The A1 replica model showed behaviour similar to the reference model although approximately 20% less resistance to slip development was observed. Additionally, the 2C replica model displayed a trend with a similar resistance to slip development of 20% less than the reference 2C model.

Both the 2C and P-T models were successfully replicated in the numerical program, and equivalent loading scenarios were applied to both of these models. Both models exhibited susceptibility to slippage when subjected to horizontal loads. Furthermore, they both demonstrated the development of gaps between the connections due to axial forces and rotational effects.

Following successful development of the Novel IMC model, equivalent loading scenarios were applied to compare its behaviour with that of the 2C and P-T models. The Novel IMC model exhibited improved resistance to all loading applications, with clear comparative behaviour observed in the single loading cases between each of the models. The Novel IMC model showed a 100% increase in resistance to slip development and bearing capacity compared to the 2C and P-T models when subjected to horizontal shear loading. Additionally, the behaviour of the Novel IMC model under axial loading significantly improved compared to both the 2C and P-T models. The 2C model did not offer any resistance to gap development under axial loading, while the P-T model suddenly failed after reaching 75 kN. In contrast, the Novel IMC model provided resistance to gap development up until 75 kN and then continued to support

the axial load up to 150 kN before experiencing plastic failure. Both the 2C and P-T models exhibited similar behaviour when subjected to applied bending or tensile axial loading, with the 2C model showing no resistance to initial displacement, and the P-T model experiencing catastrophic failure after a degradation in yield strength. In comparison, the Novel IMC model provided resistance to displacement up until approximately 2.0 kNm, at which point the model exhibited plastic deformation, doubling as a warning of a loss to structural capacity.

The improved behavioural characteristics of the Novel IMC model can be attributed to the combination of three important elements found in the 2C and P-T IMCs, including the plates, shear keys, and P-T rods. By integrating these three elements, the plates provide increased resistance to slippage and bending. The shear key enhances the bearing capacity under horizontal displacement, while the P-T rod adds tensile axial resistance and increases slip resistance.

7.3   Contributions

The Novel IMC model offers enhanced resistance to all three major types of structural loading applications. It increases resistance to slip development and bearing capacity, resulting in a 100% improvement in its response to horizontal shear force. Moreover, it provides increased resistance to gap development under tensile axial loads and bending. It also integrates redundancies to guard against catastrophic failure, thereby increasing the allowable load that can be safely applied in a real-world scenario.

Combining the geometrical elements from different IMC models has been demonstrated to enhance the performance of IMCs under various loading conditions. The design and development of an IMC is not limited to either plate-to-plate or post-tensioned systems, allowing for flexibility in design. Furthermore, potential enhancements can be achieved by amalgamating other existing design concepts to create improved connection systems and uncover other behavioural qualities.

7.4   Limitations

- The development of precise numerical models in ABAQUS in a short period of time has proven to be a challenging task. However, successful development of lower bound models was achieved, providing accurate numerical simulations to analyse and compare the behaviour between the Novel IMC model and the replica P-T and 2C models.

- The computer's processing power determines the time taken to process specific numerical tasks. Due to limited computational performance and time constraints, there was only enough time to model the behaviour of quarter sections with two columns, as opposed to half or full sections with four or eight columns, respectively.

7.5   Further Work

Due to time constraints and computational processing power limitations, further investigations into other geometrical variations of the model's design were not completed.

- Access to greater computational performance would enable more extensive research into the behaviour of half or full model sections, facilitating a better understanding of the overall behaviour of IMC models.

- Further studies, such as parametric analyses on alternative geometric variations of the Novel IMC model's design, would provide additional insights to determine the optimal design geometry.

- Conducting investigations into the development of an outer sleeve for the shear key could offer an option to minimize the gap between the shear key and the column. This could reduce the gap between the shear key and the column to at least 1 mm, thereby halving the slippage from 4 mm to 2 mm.

References

Abaqus, V. (2019) Documentation. Dassault Systemes Simulia Corporation.

Chen, Z, Liu, J, Yu, Y, Zhou, C & Yan, R 2017, 'Experimental study of an innovative modular steel building connection', *Journal of Constructional Steel Research*, vol. 139, pp. 69-82.

Dhanapal J, Ghaednia H, Das S, Velocci J 2019, Structural performance of state-of-the-art Vector Bloc modular connector under axial loads, *Engineering Structures*, vol. 183, pp. 496–509.

Dai XM, Zong L, Ding Y, Li ZX 2019, Experimental study on seismic behaviour of a novel plug-in self-lock joint for modular steel construction *Engineering Structures*, vol.181, pp. 143–64.

Farajian, M, Sharafi, P, Eslamnia, H, Kildashti, K & Bai, Y 2022, 'Classification of inter-modular connections for stiffness and strength in sway corner-supported steel modular frames', *Journal of Constructional Steel Research*, vol. 197.

Lacey, A.W., Chen, W., Hao, H. & Bi, K. 2018, "Structural response of modular buildings – An overview", *Journal of Building Engineering,* vol. 16, pp. 45-56.

Lacey, AW, Chen, W, Hao, H, Bi, K & Tallowin, FJ, 2019, 'Shear behaviour of post-tensioned inter-module connection for modular steel buildings' *Journal of Constructional Steel Research,* vol. 162.

Lacey, AW, Chen, W, Hao, H & Bi, K 2019, 'Review of bolted inter-module connections in modular steel buildings', *Journal of Building Engineering*, vol. 23, pp. 207-19.

Lacey, AW, Chen, W, Hao, H & Bi, K 2020, 'Simplified structural behaviours of post-tensioned inter-module connection for modular buildings', *Journal of Constructional Steel Research*, vol. 175.

Lacey, AW 2020, 'Structural Response of Modular Buildings to Multiple Hazards', PhD thesis, Curtin University, Perth, Western Australia

Lacey, AW, Chen, W, Hao, H & Bi, K 2020, 'Simplified structural behaviours of post-tensioned inter-module connection for modular buildings', *Journal of Constructional Steel Research*, vol. 175.

Lacey, AW, Chen, W, Hao, H & Bi, K, 2020, 'New interlocking inter-module connection for modular steel buildings: Simplified structural behaviours', *Engineering Structures*, vol. 227.

Lacey, AW, Chen, W & Hao, H 2022, 'Experimental methods for inter-module joints in modular building structures – A state-of-the-art review', *Journal of Building Engineering*, vol. 46.

Liu X, Cui X, Yang Z, Zhan, X, 2017, 'Analysis of the seismic performance of site-bolted beam to column connections in modularized prefabricated steel structures'. *Advances in Materials Science and Engineering*, vol. 2017.

Nadeem, G, Safiee, NA, Bakar, NA, Karim, IA & Nasir, NAM 2021, 'Connection design in modular steel construction: A review', *Structures*, vol. 33, pp. 3239-56.

Qin, J & Tan, P 2022, 'Design method of innovative box connections for modular steel constructions', Journal of Building Engineering, vol. 57.

Rajanayagam, H, Gunawardena, T, Mendis, P, Poologanathan, K, Gatheeshgar, P, Dissanayake, M & Corradi, M 2022, 'Evaluation of inter-modular connection behaviour under lateral loads: An experimental and numerical study', *Journal of Constructional Steel Research*, vol. 194.

Sukhi, VS, 2020, 'Seismic Mitigation of Steel Modular Buildings Using Novel Inter-Modular Connections', PhD thesis, Queensland University of Technology, Brisbane, Queensland.

Sanches, R, Mercan, O & Roberts, B 2018, 'Experimental investigations of vertical post-tensioned connection for modular steel structures', Engineering Structures, vol. 175, pp. 776-89.

Shan, S & Pan, W 2020, 'Structural design of high-rise buildings using steel-framed modules: A case study in Hong Kong', *The Structural Design of Tall and Special Buildings*. vol. 29.

Thai, H, Ngo, T & Uy, B 2020, 'A review on modular construction for high-rise buildings', *Structures,* vol. 28, pp. 1265-1290.

United Fasteners Australia 2023, Structural Assemblies, ISO Metric Coarse High Strength Structural Bolts, Property Class 8.8, viewed 5 August 2023, <https://www.unitedfasteners.com.au/media/156528/Structural-Assemblies-Technical-Information-United-Fasteners.pdf>.

Zhifeng, L, Mingpo, Z, Xing, Y, Yongshen, Z, Qiang, C, Congbin, Y, 2020, 'Changing behavior of friction coefficient for high strength bolts during repeated tightening'*, Tribology International,* vol. 151.

Appendix A

Project Specification

ENG4111/4112 Research Project

Project Specification

For: Matthew Trent

Title: Behaviour and Design of Connections in Modular Steel Buildings

Major: Civil Engineering

Supervisors: Dr Andy Nguyen (UniSQ), Tony Le (External), Sukhi Sendanayake (External)

Enrollment: ENG4111 – ONL S1, 2023

                ENG4112 – ONL S2, 2023

Project Aim: To model and investigate the behavior of two existing inter-modular connection systems. And to design, model and investigate the behaviour of a proposed novel inter-module connection system.

Programme: Version 1, 15th March 2023

1. Develop 3D connection models in AutoCAD and import into Abaqus CAE.
2. Run FEA on each of the two selected pre-existing connection models.
3. Compare and validate results with findings in the selected literature.
4. Identify and confirm the slippage and gap development problems existential in the two selected connection systems.
5. Perform FEA on the novel connection model.
6. Review and compare the results from the FEA on the novel connection system with the two pre-existing connection systems.
7. Identify the differences in slippage, gap development and any improvements or deterioration between the existing connection systems and the novel connection system.
8. Prepare and compile dissertation based on the results and differences between the pre-existing connection design with the proposed novel connection model.

Appendix B

Material Properties Calculations

General Steel Properties

$E = 200 * 10^3$ MPa, $\nu = 0.25$, $\rho = 7.85E\text{-}09$

C350 Column

$\varepsilon_u = 0.12$

$\dfrac{f_y}{E} = \dfrac{355}{200 * 10^3} = 0.001775$

Ultimate plastic strain $= \varepsilon_u - \dfrac{f_y}{E} = 0.12 - 0.001775 = 0.1182$

	Yield stress	Plastic strain
f_y 1	350	0.0
f_y 2	430	0.118

S350 Plate

$\varepsilon_u = 0.20$

$\dfrac{f_y}{E} = \dfrac{360}{200 * 10^3} = 0.0018$

Ultimate plastic strain $= \varepsilon_u - \dfrac{f_y}{E} = 0.20 - 0.0018 = 0.1982$

	Yield stress	Plastic strain
f_y 1	360	0.0
f_y 2	450	0.198

M12 Bolt

$\varepsilon_u = 0.12$

$\frac{f_y}{E} = \frac{640}{200 * 10^3} = 0.0032$

Ultimate plastic strain $= \varepsilon_u - \frac{f_y}{E} = 0.12 - 0.0032 = 0.1168$

	Yield stress	Plastic strain
f_y 1	640	0.0
f_y 2	800	0.117

R12 Loading Pin

$\varepsilon_u = 0.32$

$\frac{f_y}{E} = \frac{375}{200 * 10^3} = 0.001875$

Ultimate plastic strain $= \varepsilon_u - \frac{f_y}{E} = 0.32 - 0.001875 = 0.31813$

	Yield stress	Plastic strain
f_y 1	375	0.0
f_y 2	530	0.318

P-T Rod

$\varepsilon_u = 0.19$

$\frac{f_y}{E} = \frac{520}{205 * 10^3} = 0.00254$

Ultimate plastic strain $= \varepsilon_u - \frac{f_y}{E} = 0.19 - 0.00254 = 0.1875$

	Yield stress	Plastic strain
f_y 1	520	0.0
f_y 2	660	0.19